J. Fluid Mech. (1980), *vol.* 100, *part* 2, *pp.* 397–431
Printed in Great Britain

Controlled symmetric perturbation of the plane jet: an experimental study in the initial region

By A. K. M. F. HUSSAIN AND C. A. THOMPSON
Department of Mechanical Engineering, University of Houston, Texas 77004

(Received 4 June 1979 and in revised form 18 January 1980)

The response of the near field of a free, plane air jet (aspect ratio 44: 1) to a controlled, sinusoidal perturbation was investigated by hot-wire measurements. The experiments were carried out at an exit excitation amplitude of 1·4 % for the Strouhal number range $0{\cdot}15 \leqslant St_H \leqslant 0{\cdot}6$ and the Reynolds-number range $8 \times 10^3 \leqslant Re_H \leqslant 3{\cdot}1 \times 10^4$. The influence of the excitation, introduced with a loudspeaker attached to the jet settling chamber, on the mean and fluctuating velocity fields is much weaker than that in the circular jet. The amplitude and phase profiles of the fundamental, educed through phase-locked measurements, show that the induced symmetric mode remains symmetric as it travels downstream. The wave growth rate is much higher and the wavelength much smaller in the shear layer than on the centre-line of the jet. The wave fundamental attains its maximum amplitude at $St_H \simeq 0{\cdot}18$ on the jet centre-line and at $St_H \simeq 0{\cdot}45$ in the shear layer. The amplitude profiles of the fundamental in the shear layer agree quite well with the spatial stability theory of Michalke (1965*b*); however, the phase data do not agree well with the theoretical predictions. The growth rate and the disturbance wavenumber increase monotonically with the St_H both in the shear layer and on the centre-line but tend to approach constant values at higher St_H. The phase velocity data show that, in the lower Strouhal-number range, the plane jet acts as a non-dispersive waveguide.

1. Introduction

While the role, or even presence, of organized large-scale structures in the far fields of jets is still an open question, there is little doubt about their occurrence in the near field and even about their importance in entrainment and mixing and in aerodynamic sound generation. An investigation of the nature and role of these structures appears to be crucial for understanding the physics, as well as developing a viable theory, of shear-flow turbulence. In fact, even though the presence of large-scale eddies in turbulent shear flows had been suspected for a long time and occasionally investigated (Townsend 1956; Mollo-Christensen 1967; Payne & Lumley 1967; Hussain & Reynolds 1970), the current upsurge in the interest in the organized structures has been spurred by the relatively recent discovery of the quasi-deterministic structures in flows which otherwise would be deemed fully (random) turbulent (Brown & Roshko 1974; Winant & Browand 1974; Crow & Champagne 1971; Browand & Laufer 1975; Hussain & Zaman 1975). Regardless of whether these near-field organized motions are represented as coherent eddies or travelling waves (Moffatt 1968), attractiveness of their study

0022–1120/80/4523–1830 $02.00

stems from the expectation that an appropriate random distribution of these deterministic motions can produce a realistic theory of shear flow turbulence (Landahl 1967; Phillips 1967; Reynolds & Hussain 1972; Kovasznay 1978; Saffman 1978*a*).

For either representation of these organized motions, viz. eddies or waves, there are two alternative approaches to the study of these motions. These eddies or waves would occur and interact randomly in space and time in a natural flow (without excitation). Their detection would thus require conditional sampling or straightforward Fourier decomposition (Wills 1964; Morrison & Kronauer 1970; Clark 1979). In either case, interpretations of the results are not free from ambiguity. In fact, the educed motions and their convection velocities in the near field of a circular jet have been found to be strongly determined by whether the detection is based on positive or negative spikes in the u-signal (Lau & Fisher 1975; Bruun 1977; Yule 1978; Lau 1978, unpublished manuscript). While Wygnanski & Gutmark (1971) inferred from their correlation data that the two interfaces of an unperturbed plane jet move independently, Goldschmidt & Bradshaw's (1973) data suggested flapping of the jet.

The alternative approach is to induce the organization through controlled excitation, of the sinusoidal type (Sato 1960; Freymuth 1966; Crow & Champagne 1971; Morkovin & Paranjape 1971; Vlasov & Ginevskiy 1974; Bechert & Pfizenmaier 1975; Petersen, Kaplan & Laufer 1974; Chan 1976; Moore 1977; Hasan 1978) or the impulse type (Wygnanski, Sokolov & Friedman 1976; Cantwell, Coles & Dimotakis 1978; Sokolov *et al.* 1980; Hussain, Kleis & Sokolov 1980), and educe the organized motions through phase average measurements, locked to a specific phase of the excitation or of the induced structure signature. The latter approach is free from detection ambiguity except for some unavoidable jitter (Hussain & Zaman 1980); this approach is quite attractive because of its relative simplicity and has been extensively used in various investigations referenced in this paragraph.

The present study, completed in 1974 (Thompson 1975), focused on the wave representation of the near-exit organized motions induced by a controlled excitation, in an untripped high-Reynolds-number plane jet and followed directly on the work of Hussain & Reynolds (1970) as the logical extension. In this earlier work, involving controlled disturbances in a turbulent channel flow, it was found that the induced wave disturbances underwent rapid decay, the decay rate increasing with increasing Strouhal number. Before starting the present study, it was assumed that the induced disturbances in a plane jet would first grow downstream before undergoing decay so that data over a wide x range as well as a wide Strouhal-number range could be obtained. Thus, the data could be helpful in evaluating or formulating a wave theory of turbulence.

It was also conjectured that the plane jet response to controlled perturbation would be quite different from the then exciting, new result on the perturbed circular jet (Crow & Champagne 1971), because the interaction of the line vortices in the plane jet near field should be less energetic than that of the toroidal vortex rings in the circular jet. In addition, it was thought that since the flow in the near field was dominated by the large-scale organized motions, which in turn must depend on the initial condition (see, for example, Gutmark & Wygnanski 1976; Hussain & Zedan 1978; Clark 1979), controlled excitations might modify the large-scale structures to such an extent as to be of some technological significance. For example, controlled

excitation might produce significant changes in mixing and thus in heat, mass and momentum transfer in the near fields of jets as well as result in suppression/enhancement of aerodynamic noise production.

2. Brief literature review

The instability of initially laminar free shear layers and the formation of vortex rings in the near fields of jets had been observed and reported as far back as a century ago by researchers including Helmholtz and Rayleigh. Detailed studies of the shear-layer instability were carried out experimentally and theoretically by researchers in Berlin, and elsewhere. The linear hydrodynamic stability theory for a hyperbolic-tangent mean velocity profile of an inviscid parallel flow (Michalke 1965*b*) met with considerable success in predicting the most unstable mode, the growth rate and phase velocities of the disturbances (Freymuth 1966).

In stability studies of plane jets have been carried out theoretically by Mattingly & Criminale (1971). Spatially dependent disturbances in an inviscid, incompressible plane jet were analysed by solving the Rayleigh stability equation for the bell-shaped profile, i.e. $\mathrm{sech}^2 y$, derived from similarity of a laminar jet (Batchelor 1970). Anti-symmetric disturbances (in u) were found to have higher growth rates than the symmetric modes. With increasing Strouhal numbers St_H, the wavenumber increases monotonically for both modes while the phase velocity increases for the antisymmetric mode but decreases for the symmetric mode. For both modes, the growth rate first increases with increasing St_H at low St_H, but decreases with increasing St_H at higher St_H.

Sato (1960) experimentally investigated the instability of a plane air jet (emerging from a laminar channel flow) in the presence of an imposed transverse acoustic perturbation from a loudspeaker placed perpendicular to the flow direction. The measured Strouhal number data disagreed with the theoretical predictions for a laminar plane jet. Sato showed that, when the fluctuations were small, the unstable wavenumber, phase velocity, and growth rate agreed with the linear stability theory applied to a modified, parabolic jet profile that matches the data better than $\mathrm{sech}^2 y$. Sato found that, for the Reynolds number $Re_\theta (\simeq U_e\theta/\nu)$ range 80–500, the most sensitive Strouhal number $St_\theta (\equiv f\theta/U_e)$ of the laminar jet fell in two distinct ranges: the St_θ was about 0·015 for symmetric modes and about 0·009 for antisymmetric modes. However, the most unstable jet Strouhal number St_H was constant ($St_H = 0{\cdot}23$ for symmetric modes and $St_H = 0{\cdot}14$ for antisymmetric modes) only when the jet Reynolds number was small, but increased to values as high as $St_H \simeq 1{\cdot}5$ at higher Reynolds numbers ($Re_H \simeq 4 \times 10^4$).

Beavers & Wilson (1970) observed that the near field of a plane jet consisted of periodic motions, the natural breakdown process was essentially symmetric for small Re_H, and the instability and vortex formation were very sensitive to external disturbances. Rockwell & Niccolls (1972) found that the growth of natural disturbances in a plane jet at low Re_H was a strong function of the initial condition. At higher Re_H, the motions cycled between symmetric and antisymmetric modes. Rockwell (1972) also visualized a plane water jet under transverse excitations. Goldschmidt & Kaiser (1971) studied a plane air jet under the influence of transverse acoustic excitation and

found that the jet widening rate, geometric virtual origin, and decay rate were quite sensitive to the frequency of excitation, even though the similarity of the flow field was maintained. They also observed that the excitation caused a reduction in intermittency (but an increase in the intermittency factor) near the edge of the jet. Morkovin & Paranjape (1971) explored shear-layer oscillations induced by external sound sources in various configurations and conjectured that the 'acoustic coupling' of the instability mechanism resulted from the dependence of the velocity perturbation on the transverse pressure gradient near the detachment line.

This paper reports the first study of the response of a high-Reynolds-number plane jet (with a top-hat exit profile) to controlled symmetric perturbations.

3. Apparatus and procedures

A plane jet facility discharging air through a $3{\cdot}18 \times 140$ cm (i.e. $1\frac{1}{4}$ in. $\times$ 55 in.) slit was built for this study. The vertical slit was located between the ceiling and the floor and between the two side walls of the $30 \times 15 \times 3{\cdot}5$ m laboratory. The facility consists of a series of independently replaceable wooden modules connected together with flexible rubber sheets in order to minimize transmission of vibrations. The entire blower–motor assembly simply rested on the floor through neoprene isolators, thus providing the necessary isolation of the assembly from the laboratory floor.

Air from the blower enters the wide-angle rectangular diffuser (of angles 22° and 24°) after passing through a 1·3 m long straightener box. Four screens (10 mesh/cm, 33 % solidity) were installed in the 2·34 m long diffuser box in a novel way so as to suppress flow separation inevitable at these large diffuser angles and to uniformize the mean velocity distribution across the diffuser exit plane. Each stainless screen was cut about 2 cm smaller than the interior dimension of the corresponding location in the diffuser, was spot welded onto a thin (1 mm diameter) stainless steel wire frame and then stretched taut in position through diagonal wires tightened from outside the diffuser frame. This method eliminated the necessity of interrupting the formica-lined (for heated experiments) smooth interior surface of the diffuser as well as the cumbersome flange connexion that would be required in the conventional mounting of the screens. A uniform gap of about 1 cm, thus provided all around each screen, produced a wall jet-like flow between the diffuser and the perimeter of each screen and thus further suppressed flow separation within the diffuser. The 2 m long 140×140 cm settling chamber was also installed with four screens.

The two-dimensional nozzle was built in house using the cubic equation contour (Hussain & Ramjee 1976) and following an elaborate construction procedure (Thompson 1975). The 2 m long nozzle of a contraction ratio of 44:1 is lined with formica. In order to better define the initial boundary condition of the plane jet, end plates were mounted flush with the exit such that the slit is located at the middle of a 2×2 m exit plate, and the flow emerges normal to it. In order to prevent separation of the entrainment-induced boundary layer on the end plates, their leading edges were fitted with 8 cm diameter circular cylinders (figure 1).

Especially because of the modular design, rubber connexions, isolation of the blower–motor assembly and heavy build of the facility, the nozzle is free from any

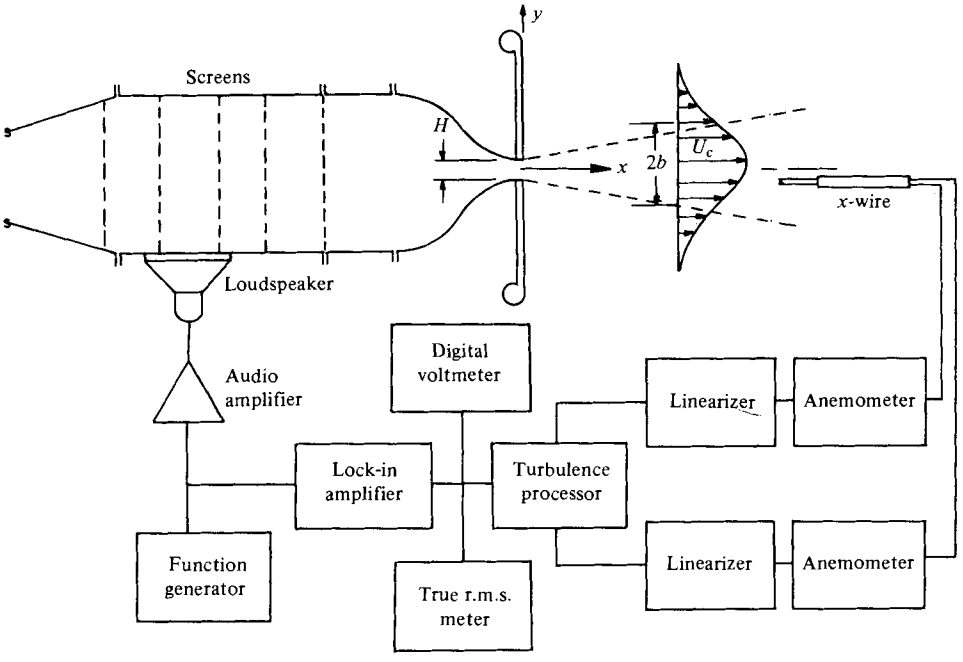

FIGURE 1. Schematic diagram of the flow and instrumentation.

perceptible vibration. Any flow oscillation detected must, thus, originate from tunnel cavity resonances or the induced controlled excitation. The vertical plane jet of aspect ratio 44:1 discharges into a large ($13 \times 15 \times 3{\cdot}5$ m) space in the laboratory with controlled temperature, humidity and traffic; thus, the turbulence level in the ambient air is not likely to be significant (Kotsovinos 1976; Bradshaw 1977).

An 8 Ω, 60 W Jensen loudspeaker was attached airtight to one side of the settling chamber through a 15 cm hole located immediately downstream from the diffuser and was driven to excite the settling-chamber cavity resonance modes of the tunnel. A second speaker attached to the chamber failed to increase the available exit excitation level and thus was not used any further. A sinusoidal signal from a function generator was amplified in an audio amplifier before it was fed to the speaker.

Velocity measurements were made using single and X-probe tungsten hot wires of 4 μm diameter, 2 mm long, at a resistance ratio of 1·4. Linearized signals from the DISA constant-temperature anemometers (55 M System) were analysed by a turbulence processor (DISA 52B25), digital voltmeters (DISA 55D31), and true r.m.s. meters (DISA 55D35). The r.m.s. amplitude and phase of the fundamental component in the velocity signal in the jet were determined by a Two Phase/Vector Lock-in-Amplifier (PAR 129A), to which the function generator driving the speaker provided the reference signal (figure 1). The display meters on the lock-in amplifier, when operated in the 'vector operation' mode, directly provided the r.m.s. amplitude of the fundamental at the disturbance frequency and its phase (in degrees) with respect to the reference wave. The accuracy of the lock-in-amplifier was checked with a synthetic signal consisting of a mixture of a random noise and a sine wave of known

amplitudes and phases. The wave-amplitude accuracy was about $\pm 5\,\%$ of peak values and phase angle accuracy was within $\pm 10°$. The x-wire was used only for transverse velocity measurements.

4. Results and discussion

(*a*) *General jet response*

While driving the speaker with the function generator, careful sweep through a wide frequency range showed that the settling-chamber cavity could be excited only at a few discrete frequencies, viz. 70 Hz, 278 Hz and 358 Hz. However, the available exit excitation amplitude progressively decreased with increasing frequency so that the 70 Hz excitation presented itself as the only realistic choice. Experiments were thus carried out with excitations at this frequency. Since at this frequency the acoustic wavelength is nearly two orders of magnitude larger than the jet slit width, the induced acoustic perturbation in the jet can be considered to be symmetric and was experimentally checked to be so. Data were obtained at the Strouhal numbers St_H ($\equiv fH/U_e$) of 0·15, 0·18, 0·25, 0·3, 0·36, 0·4, 0·45, 0·5 and 0·6 by varying the exit velocity U_e; H is the jet slit width. The corresponding exit Reynolds numbers Re_H, exit momentum thicknesses θ_e, and the momentum thickness Strouhal number $St_{\theta e}$ are listed in table 1. Data were not taken at higher Strouhal numbers because the corresponding exit velocities would be small enough that the effects of the ambient air draughts and turbulence could not be considered negligible.

In order to carry out the controlled experiment, it was decided to study the jet response to excitations at different St_H with all the other parameters held constant. While the Reynolds number had to be changed in order to vary the St_H, it was decided to carry out the experiment with excitations of a fixed exit amplitude. However, for a fixed excitation frequency and power input to the speaker, the relative exit forcing amplitude u'_{fe}/U_e increased as St_H was increased. While higher exit forcing amplitudes could be achieved at the highest St_H, the maximum forcing available at $St_H = 0{\cdot}15$ was $1{\cdot}4\,\%$. (Subsequently, by enclosing the speaker in an air-tight box outside the settling chamber, it was possible to increase the excitation amplitude to $2{\cdot}5\,\%$. However, in order to keep the excitation level as small as possible, and thus enable comparison of the data with the linear theory, this higher amplitude was not used.)

Even though data have been taken for the St_H range 0·15–0·6, detailed amplitude and phase profiles were measured at two St_H only, viz 0·18 and 0·3. These two Strouhal numbers were chosen for detailed experimentation on the basis of the following reasons: (i) the fundamental reaches the maximum amplitude on the centre-line of our plane jet at $St_H = 0{\cdot}18$, while (ii) $St_D = 0{\cdot}3$ was found to be the '*preferred*' *mode* for a circular jet (Crow & Champagne 1971; Hussain & Zaman 1975). Figures 2(*a*, *b*) show the streamwise distributions of the r.m.s. fundamental u'_f/U_e along the centre-line at a few u'_{fe}/U_e (indicated as percentages) for $St_H = 0{\cdot}18$ and 0·3, respectively. Note that the jet response increases with increasing excitation amplitudes until saturation is reached. Thus, in order to keep the excitation amplitude small as well as constant at all St_H, u'_{fe}/U_e was held constant at $1{\cdot}4\,\%$ for all the data reported here.

St_H	$Re_H \times 10^4$	θ_e (cm)	$St_{\theta e}$
0·15	3·16	0·0218	0·0010
0·18	2·67	0·0236	0·0013
0·25	1·93	0·0269	0·0021
0·30	1·61	0·0315	0·0030
0·35	1·34	0·0356	0·0040
0·40	1·20	0·0406	0·0051
0·45	1·10	0·0429	0·0061
0·50	0·96	0·0434	0·0068
0·60	0·80	0·0457	0·0086

TABLE 1. Jet excitation conditions.

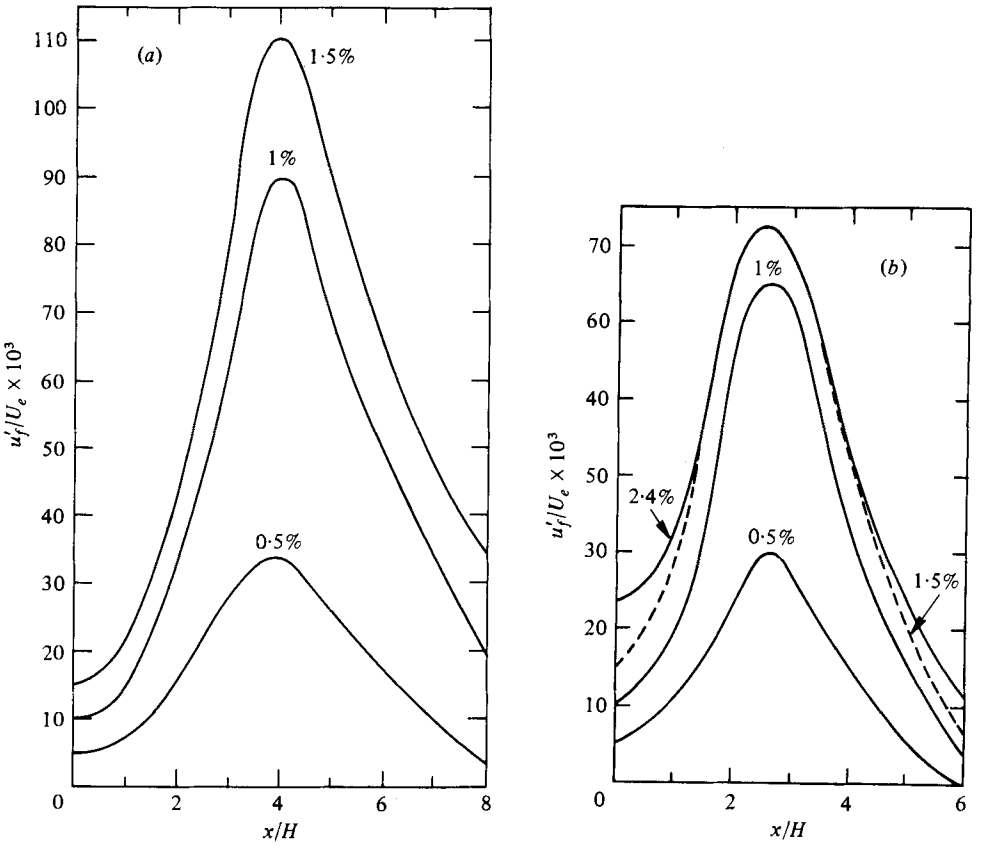

FIGURE 2. The response of the jet centre-line $u_f'(x)$ to the exit excitation amplitude: (*a*) $St_H = 0{\cdot}18$; (*b*) $St_H = 0{\cdot}30$.

(*b*) *Basic flow and influence of controlled perturbation*

Since data in this study were limited to the centre-height and the first few slit widths only, the flow can clearly be regarded as homogeneous in the spanwise direction. Experiments reported in this paper were performed without the jet-confining plates. Subsequently, confining plates have been added. All data reported here were retaken

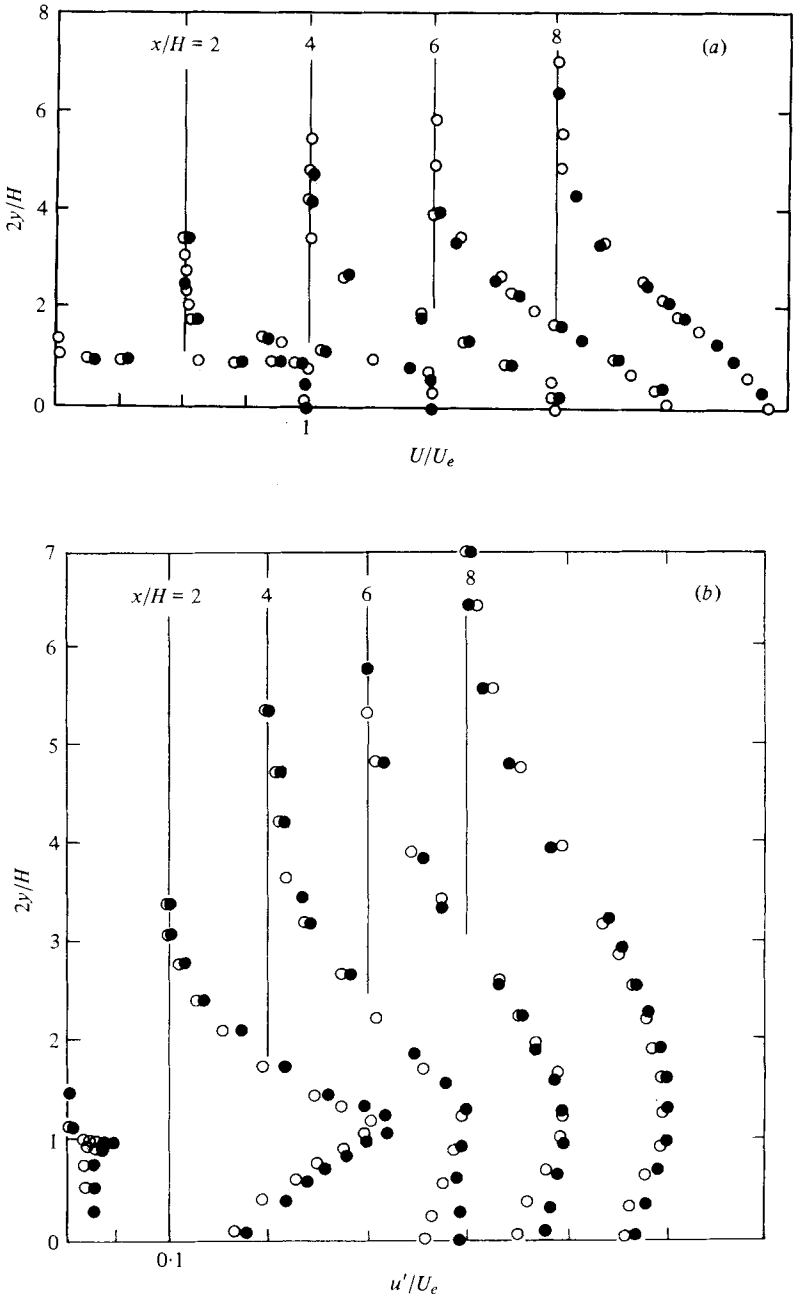

FIGURE 3. Response of the jet mean and turbulent velocity profiles to the perturbation: ○, unexcited; ●, excited at $St_H = 0{\cdot}18$. (*a*) Mean velocity; (*b*) longitudinal turbulence intensity.

and were found to duplicate the original data well within the experimental uncertainty. For all the studies reported here, the exit mean velocity profile, both with and without the small-amplitude velocity perturbation, agreed very closely with the Blasius profile.

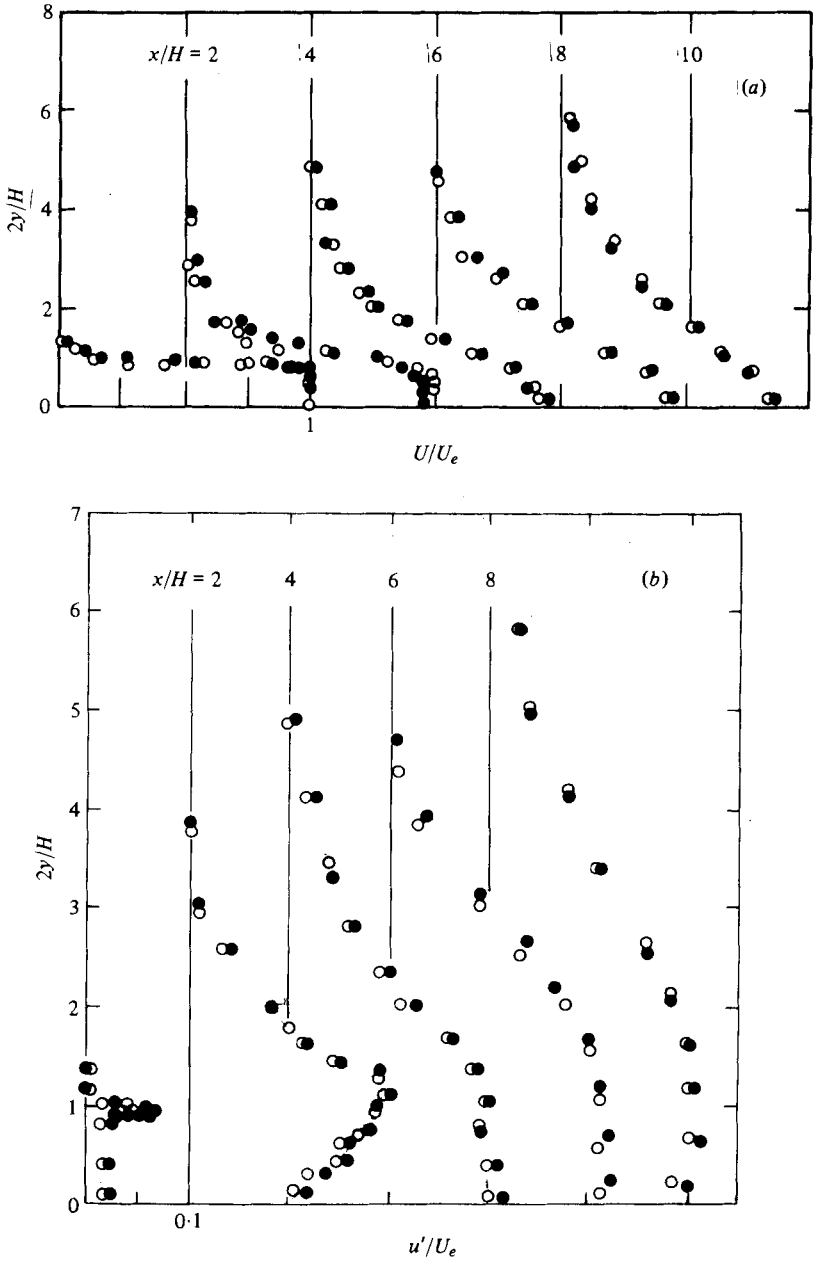

FIGURE 4. Response of the jet mean and turbulent velocity profiles to the perturbation: ○, unexcited; ●, excited at $St_H = 0{\cdot}30$. (*a*) Mean velocity; (*b*) longitudinal turbulence intensity.

Even though transverse (y) traverses were made at a number of x stations at $St_H = 0{\cdot}18$ and $0{\cdot}30$, detailed data were acquired only on the jet centre-line (i.e. line of symmetry) and along the shear layer (i.e. along the line where the mean velocity is half of the local maximum velocity). For brevity, *these two planes will be designated as CL and SL*, respectively.

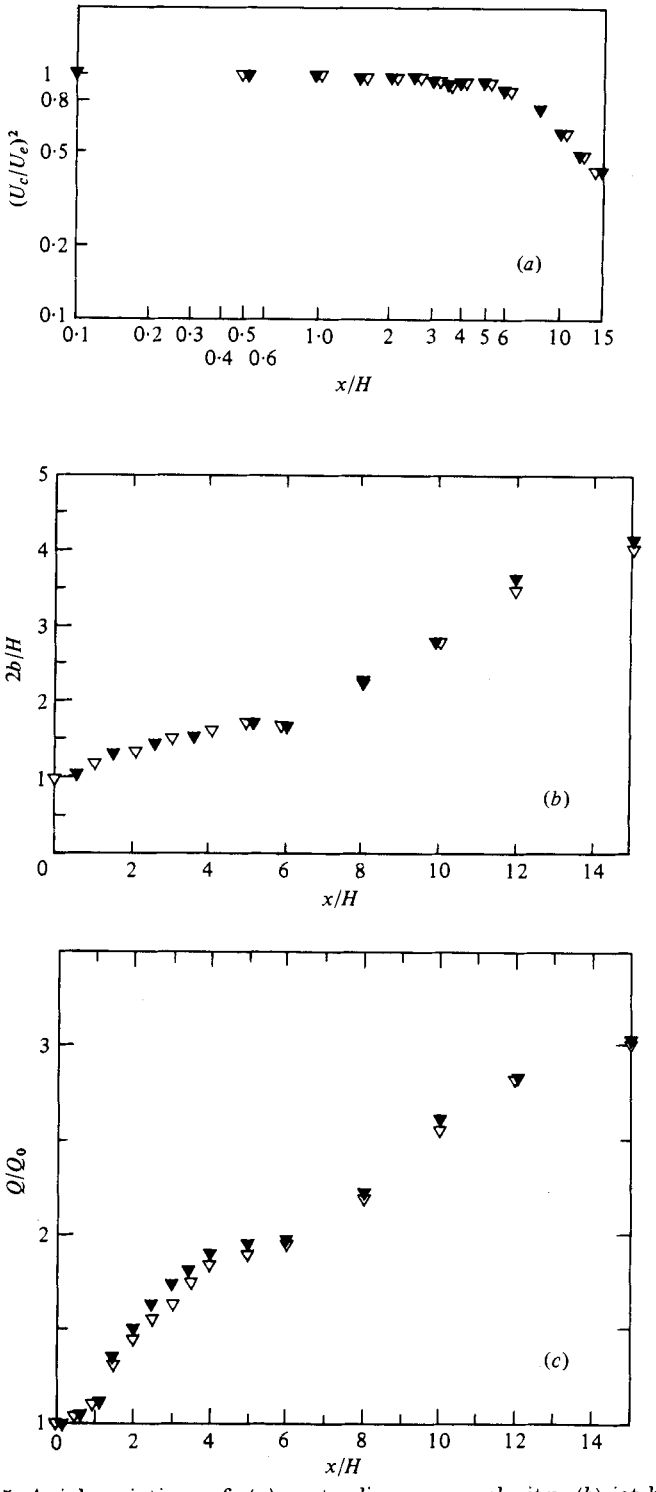

FIGURE 5. Axial variations of: (*a*) centre-line mean velocity; (*b*) jet half-width; (*c*) mass flux. ▽, unforced; ▼, forced at $St_H = 0{\cdot}18$.

The longitudinal mean velocity and turbulent intensity profiles with and without excitation are shown in figures 3 and 4 for $St_H = 0{\cdot}18$ and $0{\cdot}3$, respectively. The effect on the mean field is clearly marginal. The effect of transverse acoustic excitation on a laminar plane jet was also found negligible except at the outer edges (Sato 1960). The effect of controlled excitation on $U(y)$ in a circular jet was also found to be negligible, even though noticeable differences were found in the entrainment rate (Crow & Champagne 1971; Hussain & Zaman 1975). The effect of the excitation appears to be more significant on the fluctuation intensity and is more pronounced on the CL than in the SL. Circular jet data also show a comparable effect of controlled excitation.

Figures 5 (*a*, *b*) show the streamwise variations of the centre-line longitudinal mean velocity U_c and the half-width b (corresponding to the transverse location of $\frac{1}{2}U_c$ in the mean profile $U(y)$), respectively, at $St_H = 0{\cdot}18$. The effect of excitation is not clearly discernible in the mean quantities, thus suggesting that the response of the plane jet to controlled perturbations is distinctly different from that of the circular jet. The point of sharp drop in $(U_c/U_e)^2$ or rise in $b(x)$ corresponds to the 'transition point' identified by Sato (1960) and occurs at $x/H \simeq 5{\cdot}5$. The corresponding point in the circular jet is at $x/D \simeq 4$. Figure 5 (*c*) shows the streamwise variation of the normalized mass flux

$$Q/Q_e = 2\left[\int_0^\infty U\,dy\right]\Big/U_eH.$$

In a circular jet (Crow & Champagne 1971; Hussain & Zaman 1975), the mass flux is noticeably higher when excited. If vortex-pairing phenomenon is responsible for entrainment, i.e. engulfment (Winant & Browand 1974), these data suggest that vortex pairing in the near field of the circular jet is considerably more dominant than in the plane jet. Of course, for equal sizes of the diameter and the slit-width, because of much larger turbulent/nonturbulent interface area in the case of the circular jet, the circular jet entrainment and mixing rate should be expected to be higher than the plane jet. From the mass flux $Q(x)$ data, the streamwise variation of the computed non-dimensional entrainment rate $E_n(x) = d(Q/Q_e)/d(x/H)$ shows that $E_n(x)$ increases rapidly to a maximum of about $0{\cdot}36$ at $x/H \simeq 1{\cdot}7$, then rapidly decreases until at $x/H \simeq 3$ before slowly decreasing further to the value of about $0{\cdot}08$ at $x/H \simeq 14$. The far-field entrainment rate in a circular jet has been found to be about $0{\cdot}32$ (Ricou & Spalding 1961; Hill 1972), and large variations in $E_n(x)$ can be achieved with small-amplitude controlled perturbations (Crow & Champagne 1971; Zaman & Hussain 1980).

The total mean streamwise momentum fluxes

$$MT(x) \equiv \int_{-\infty}^{\infty} \rho(U^2 + \overline{u^2})\,dy$$

for both excited and unexcited cases are shown in figure 6 (*a*) and the mean momentum fluxes due to the longitudinal turbulence, i.e.

$$MF(x) \equiv \int_{-\infty}^{\infty} \rho\overline{u^2}\,dy$$

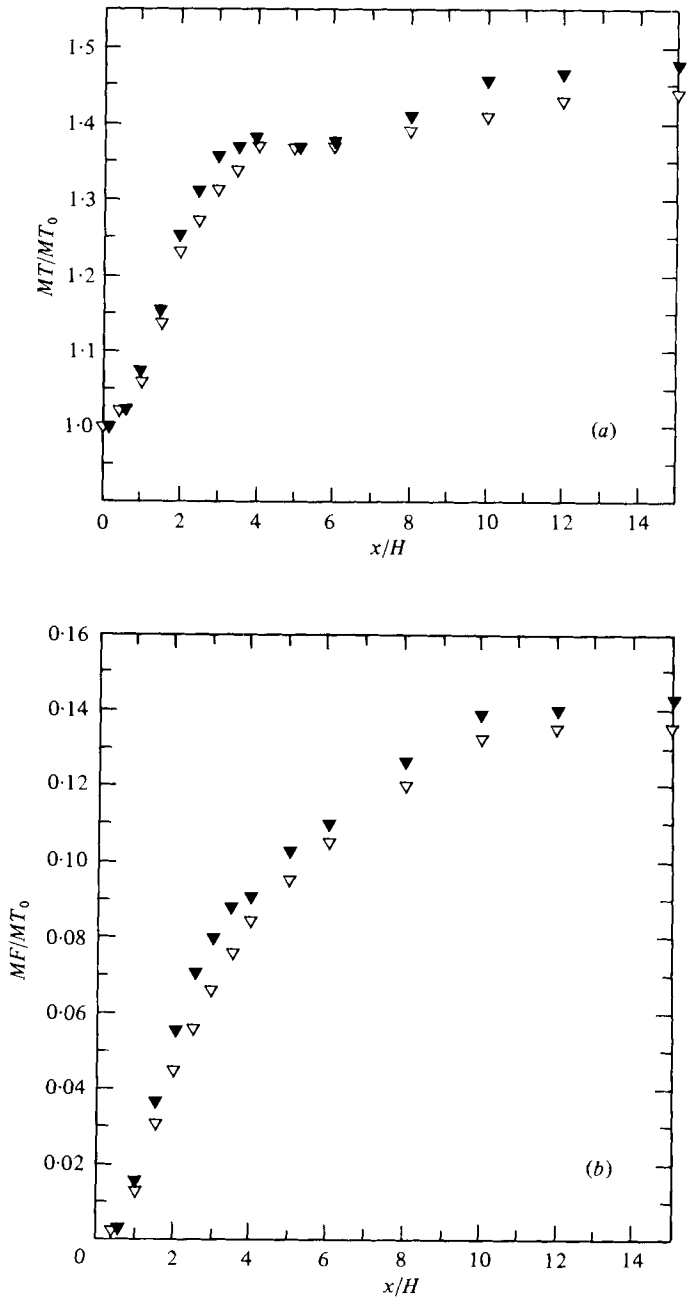

FIGURE 6. Axial variations of: (*a*) $MT(x)$; (*b*) $MF(x)$. For legend see figure 5.

for both perturbed and unperturbed cases are shown in figure 6 (*b*). Note that the mean momentum flux in a jet increases first rapidly and then gradually. Notwithstanding the prevalent and widespread claims to the contrary, the streamwise increases of the momentum flux are real and have been conclusively demonstrated and explained on the basis of negative mean static pressure in turbulent jets, the negative pressure being

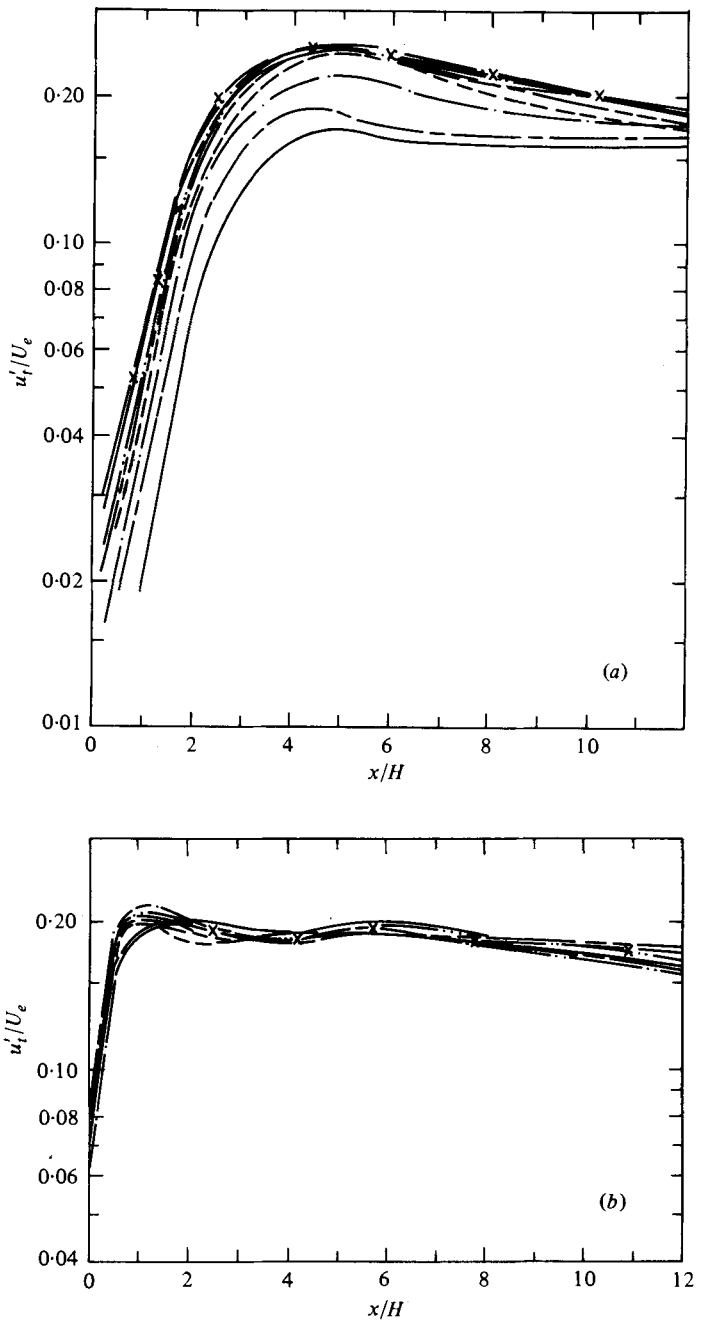

FIGURE 7. Axial variations of u_t' at different St_H: (*a*) CL; (*b*) SL. ——, $St_H = 0{\cdot}15$; — - —, $St_H = 0{\cdot}18$; — · —, $St_H = 0{\cdot}25$; - - - -, $St_H = 0{\cdot}30$; — - - —, $St_H = 0{\cdot}36$; — · · —, $St_H = 0{\cdot}40$; — · · · —, $St_H = 0{\cdot}45$; — - · —, $St_H = 0{\cdot}50$; — × —, $St_H = 0{\cdot}60$.

supported by transverse turbulent velocity fluctuations (Hussain & Clark 1977). Streamwise increases of the momentum flux have been observed also in the circular jet (Kleis 1974). Figure 6(*b*) shows that the fluctuating field contributes to about 15 %

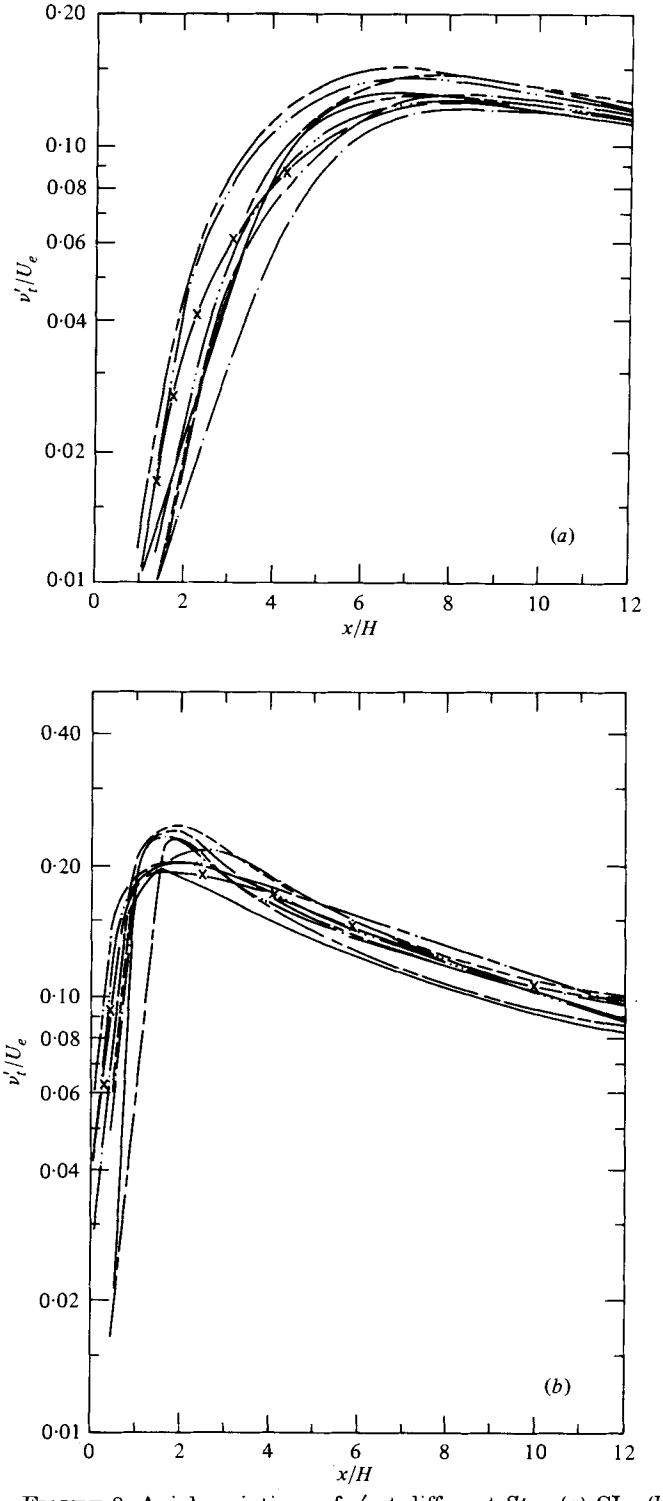

FIGURE 8. Axial variations of v_t' at different St_H: (*a*) CL; (*b*) SL. For legend see figure 7.

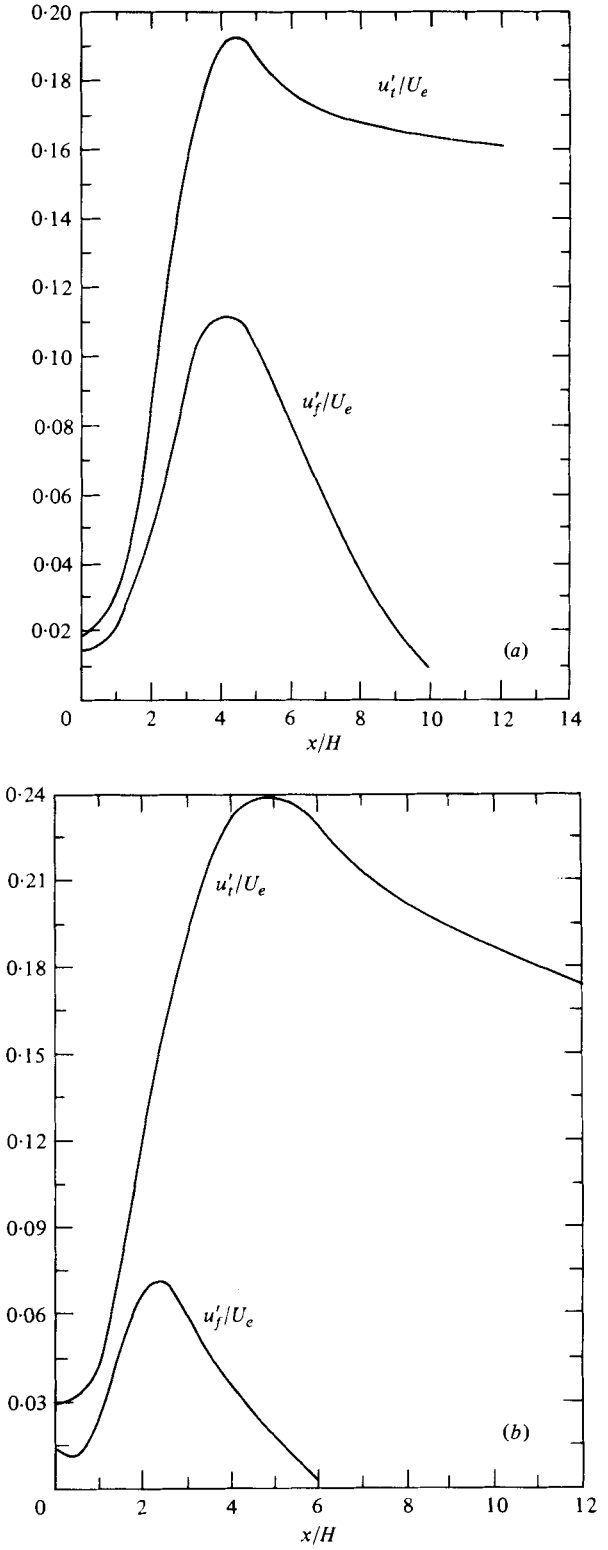

FIGURE 9. Axial variations of u_t' and u_f' on the CL: (*a*) $St_H = 0{\cdot}18$; (*b*) $St_H = 0{\cdot}30$.

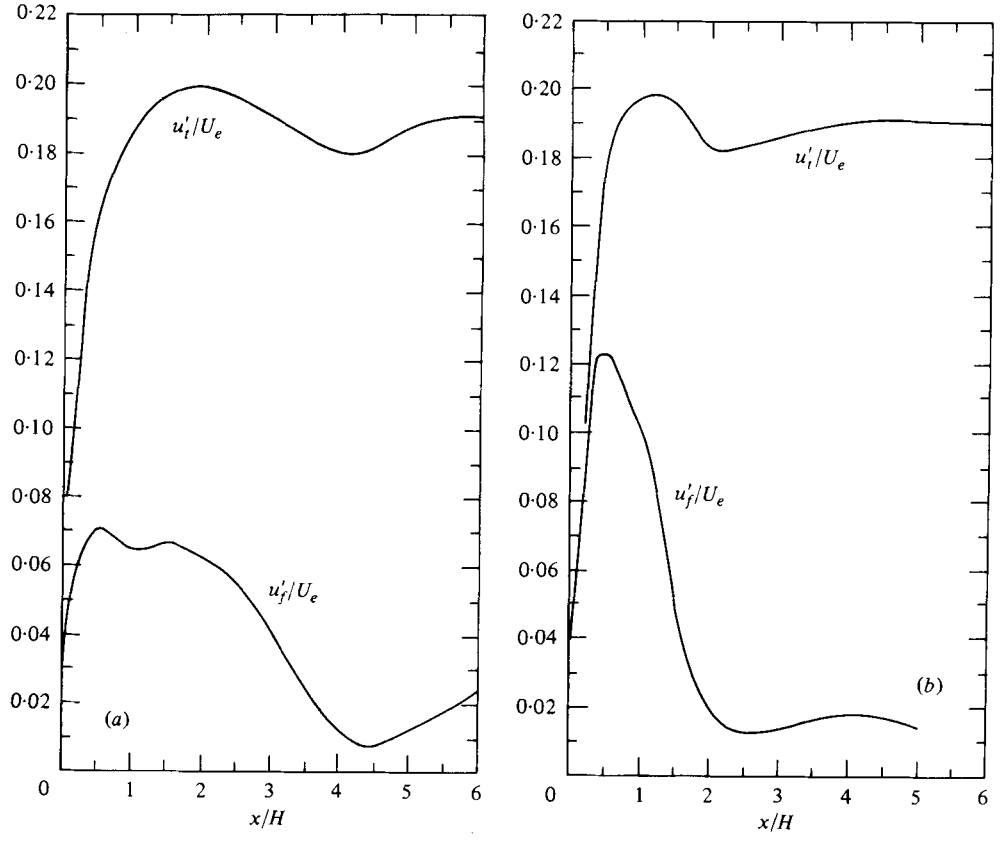

FIGURE 10 (*a*,*b*). For legend see next page.

of the total far-field average momentum fluxes. Note that effects of the controlled perturbation are more noticeable on MT and MF than on the other integral measures like U_c, b, Q or E_n.

Figures 7 (*a*, *b*) show that the growth rate of the total longitudinal turbulence intensity u_t'/U_e is higher in the SL than on the CL. The SL data appear independent of St_H while the CL data show small but systematic dependence on St_H. The maximum value of u_t'/U_e occurs at $x/H \simeq 1$ in the SL and at $x/H \simeq 4$ on the centre-line, both values being approximately equal. The growth appears exponential both in the SL and on the CL, the growth rate in the SL being somewhat higher than that on the CL. The oscillation in the u_t' data in the SL will be explained later in terms of the fundamental amplitude variation $u_f'(x)$.

Figures 8 (*a*, *b*) show the streamwise variations of the transverse r.m.s. intensities $v_t'(x)$ on the CL and in the SL, respectively. Because of the averaging effect of the x-wire, the accuracy of the $v_t'(x)$ data, especiallynear the jet exit, will be lower than $u_t'(x)$. Like the $u_t'(x)$ data, $v_t'(x)$ also rises more rapidly in the SL than on the CL. However, the peak value of v_t' is much higher in the SL, and the peak on the CL occurs farther downstream, i.e. at $x/H \simeq 7$ as opposed to $x/H \simeq 4$ for $u_t'(x)$. Thus, in the SL, $\overline{v_t^2}/\overline{u_t^2}$ exceeds 1 at the location ($x/H \simeq 1$) of the peak values while, on the CL, this ratio

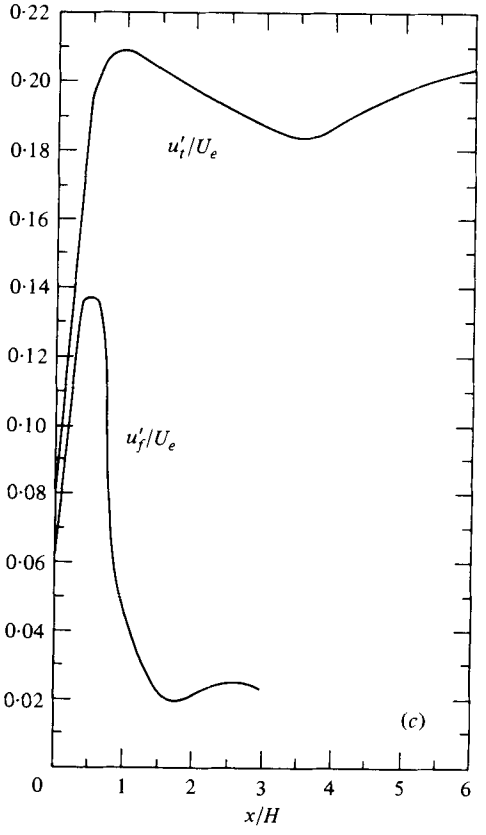

FIGURE 10. Axial variations of u_t' and u_f' in the SL: (*a*) $St_H = 0{\cdot}18$; (*b*) $St_H = 0{\cdot}30$; (*c*) $St_H = 0{\cdot}45$.

is always less than 1. Such high values of $\overline{v_t^2}/\overline{u_t^2}$ in the SL has also been observed, though not explained, by P. Bradshaw (1979, private communication).Comparatively large transverse velocities during the shear-layer roll-up can produce large values of $\overline{v_t^2}/\overline{u_t^2}$. In fact, induction of orderly vortex roll-up and pairing through controlled excitation in a circular jet has been shown (Zaman & Hussain 1980) to produce values of $\overline{v_t^2}/\overline{u_t^2}$ exceeding 1. For detailed discussion of the possible effects of flow reversal near the outer edges of the jet, see Hussain & Zaman (1980) and Antonia, Chambers & Hussain (1980).

The essentially negligible sensitivity of the total turbulence intensity in a plane jet to the controlled perturbation indicates that the plane jet response to perturbations is much weaker than that of the circular jet. Figures 9(*a*, *b*) compare the fundamental r.m.s. amplitudes $u_f'(x)$ with the total $u_t'(x)$ on the CL at $St_H = 0{\cdot}18$ and 0·30, respectively; and figures 10(*a*, *b*, *c*) in the SL at $St_H = 0{\cdot}18$, 0·30 and 0·45, respectively. In the plane jet, u_f' is much smaller than u_t'. In the circular jet, on the other hand, the $u_f'(x)$ and $u_t'(x)$ are comparable; at $St_D \simeq 0{\cdot}3$, u_f' is within 97 % of u_t'; this St_D is thus called the 'preferred mode' of the circular jet. [It has been subsequently demonstrated (Zaman & Hussain 1980) that the jet centre-line fluctuation intensity can reach extremely high values under the conditions of enhanced pairing. The $St_D \simeq 0{\cdot}3$,

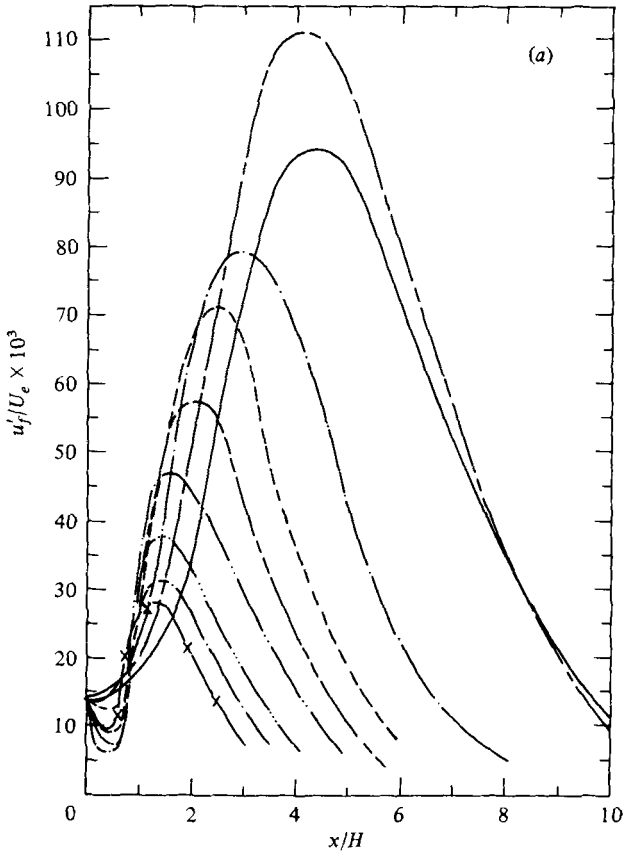

FIGURE 11(a). For legend see next page.

defined as the 'preferred mode' based on the u_t' data by Crow & Champagne (1971), can still be called the preferred mode if redefined to be based on the fundamental amplitude only.] In the plane jet, the maximum value of u_f' is reached at $St_H \simeq 0{\cdot}18$ on the CL and at $St_H \simeq 0{\cdot}45$ in the SL. At either St_H, the u_f' peaks are relatively much weaker than u_t' peaks. In this sense, the plane jet can be said to have no strong 'preferred mode', at least for symmetric perturbations.

(c) *Wave data and analysis*

Figures 11 (*a*, *b*) give the distributions in x of the fundamental amplitudes u_f'/U_e at various St_H on the CL and in the SL, respectively. On the CL, the fundamental amplitude increases exponentially before reaching the peak values; the growth rate monotonically increases with St_H, the increase progressively becoming smaller at higher St_H. The decay rate appears to be independent of the St_H. The peak value of u_f'/U_e monotonically decreases with increasing St_H and its location progressively moves upstream with increasing St_H. Figure 11 (*c*) shows the location of the peak of $u_f'(x)$ with St_H. The circular jet data (Crow & Champagne 1971; Zaman & Hussain 1980) show similar trend with St_D and also show a levelling-off of the growth rate with

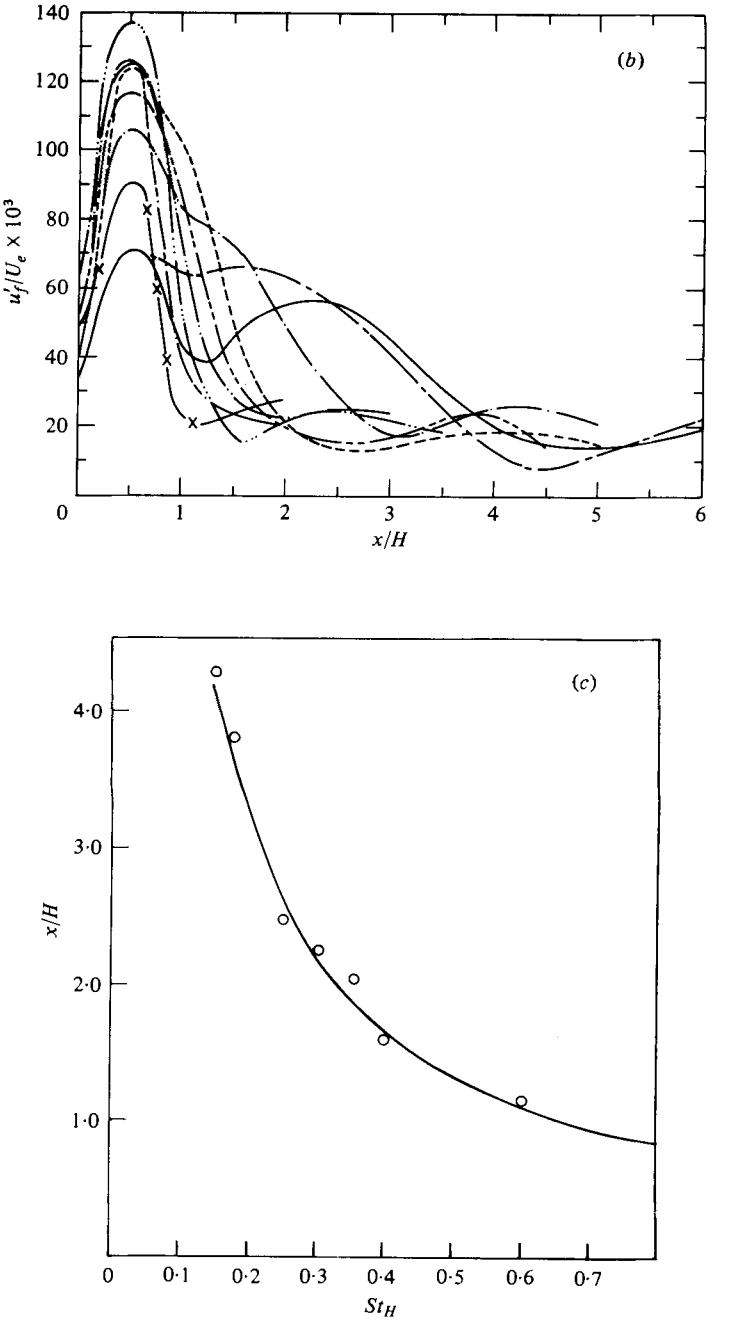

FIGURE 11. Axial variations of u_f' at different St_H on (*a*) the centre-line and (*b*) the shear layer. For legend see figure 7. (*c*) Locations of peaks of $u_f'(x)$ on the centre-line.

St_D. The dependence of the location of occurrence of the peak value of $u_f'(x)$ on the Strouhal number should serve as a warning against identifying the preferred mode based on data obtained at a fixed x (Crow & Champagne 1971).

In the SL, the growth rate of u_f' increases with St_H also but, above $St_H \simeq 0{\cdot}36$, the

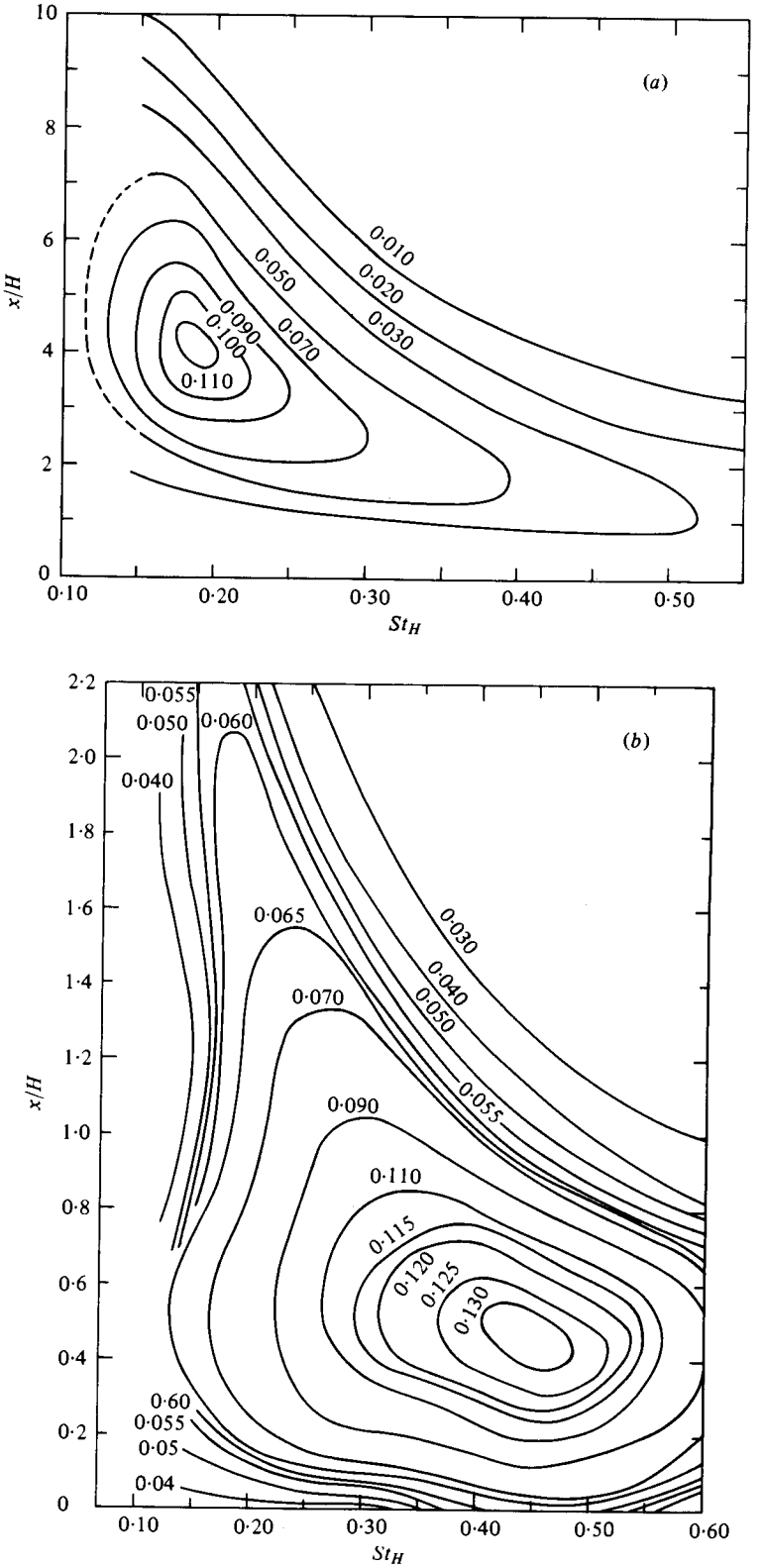

FIGURE 12. Contour map of u'_f/U_e: (*a*) CL; (*b*) SL.

increases at higher St_H appear marginal. Freymuth's (1966) data also showed that the growth rate in the laminar shear layer increases with $St_{\theta e}$. His data range covered $0{\cdot}0034 \leqslant St_{\theta e} \leqslant 0{\cdot}0218$ and $0 \leqslant x/\theta_e \leqslant 100$. In our case, these ranges are

$$0{\cdot}001 \leqslant St_{\theta e} \leqslant 0{\cdot}0086 \quad \text{and} \quad 0 \leqslant x/\theta_e \leqslant 800.$$

The oscillations downstream from the peak can be attributed to vortex pairing. The present data were taken at comparatively large x intervals, but the relation of the u_f' oscillations to vortex pairing was explained in a subsequent study in the mixing layer of a round jet (Zaman & Hussain 1980).

Figures 12 (*a*, *b*) show contour maps of constant levels of u_f'/U_e on the CL and in the SL, respectively, in the $(St_H, x/H)$ co-ordinates. The maximum response on the CL occurs at $St_H \simeq 0{\cdot}18, x/H \simeq 4$, while that in the SL occurs at $St_H \simeq 0{\cdot}45, x/H \simeq 0{\cdot}5$. These differences between the SL and CL are to be expected. Note that Crow & Champagne (1971) obtained u_f' data using a narrowband filter which thus contained phase-random contribution at the bandpass frequency. Our data were obtained with a phase-lock amplifier and, thus, are more relevant for comparison with theoretical predictions.

Figures 13 (*a*, *b*) show the streamwise variations of the transverse fundamental r.m.s. amplitude v_f' on the CL and the SL, respectively. Note that the amplitudes on the CL are about an order of magnitude smaller than those in the SL. Consequently, the CL data are likely to be less reliable than those in the SL. The lower amplitudes on the CL as opposed to those in the SL is consistent with a symmetric mode of disturbance in the plane jet.

Figures 14 (*a*, *b*) show the streamwise variations of the phase $\phi_u(x)$ of the fundamental of the longitudinal velocity perturbation $u_f(x)$ on the CL and in the SL, respectively. Closer to the exit, the ϕ_u data do not vary with x linearly, this region being the region of the adjustment of the nozzle flow to the unbounded flow and may be associated with the amplitude dips (at $x \simeq 0{\cdot}5H$) in figure 11 (*a*). Only the linear range of variation of $\phi_u(x)$ has been included. The vertical bar on each line indicates data uncertainty. Note that the x range of the data in the SL is lower than that on the CL, that uncertainty in the ϕ_u increases somewhat with x, and that this uncertainty in the SL is larger than that on the CL. The linear variation of $\phi_u(x)$ is consistent with the wave representation of the fundamental.

Figures 15 (*a*, *b*) show the streamwise evolutions of the profiles of the longitudinal perturbation fundamental amplitude u_f' for $St_H = 0{\cdot}18$ and $0{\cdot}30$, respectively. Figures 16 (*a*, *b*) show the corresponding phase profiles, respectively. The local jet half-width $b(x)$ has been used to non-dimensionalize the transverse co-ordinate y. Note that both the amplitude and phase profiles are symmetric with respect to the jet centre-line, a fact consistent with negligible v_f' on the CL as opposed to those in the SL. Note that the amplitude initially grows much faster in the SL than on the CL.

A better picture of the disturbance propagation can be obtained by plotting contours of constant phase, as shown in figure 16 (*c*). Note that the disturbance propagates initially only in the shear layer, being driven by the shear. Further downstream, say at $x/H \simeq 3{\cdot}5$, the disturbance on the centre-line starts to lead that in the shear layer.

In order to compare the data with Michalke's (1965*b*) spatial stability theory, the data at $x/H = 1$ was chosen for comparison. This station was chosen because it was

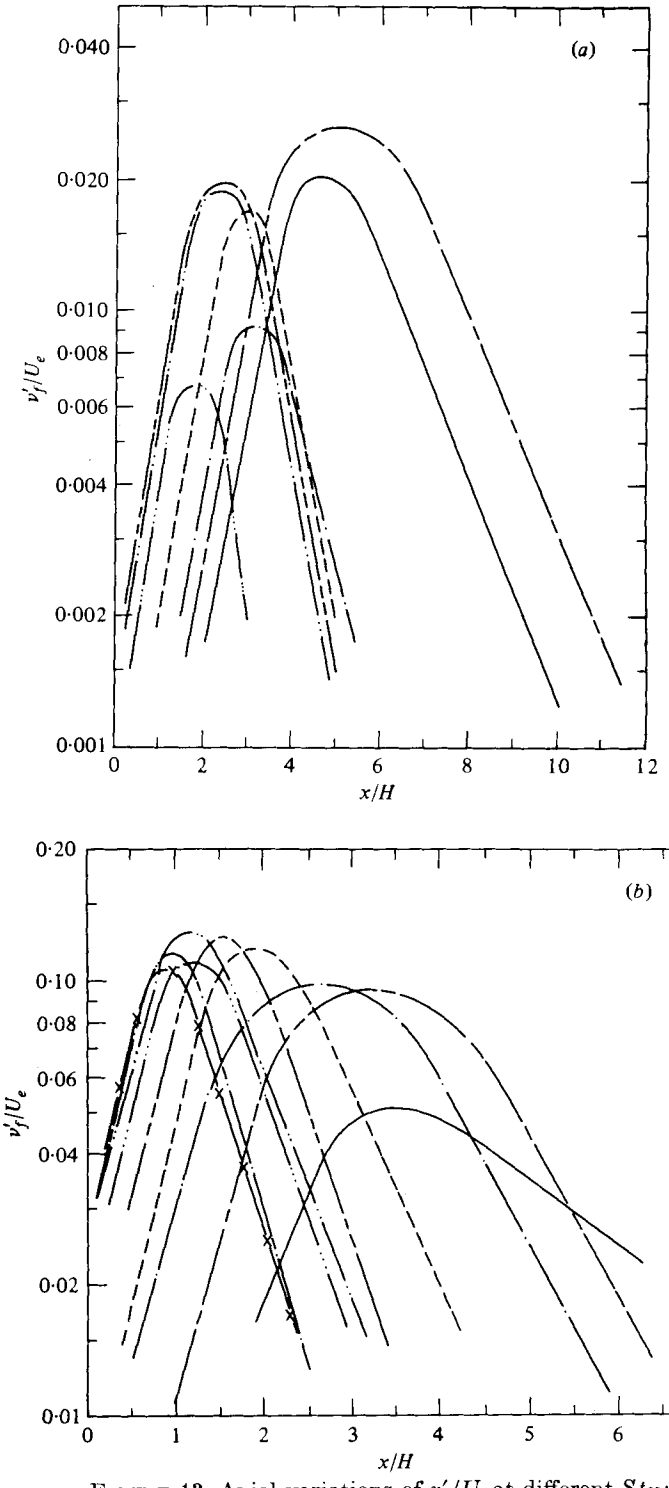

FIGURE 13. Axial variations of v_f'/U_e at different St_H: (*a*) CL; (*b*) SL. For legend see figure 7.

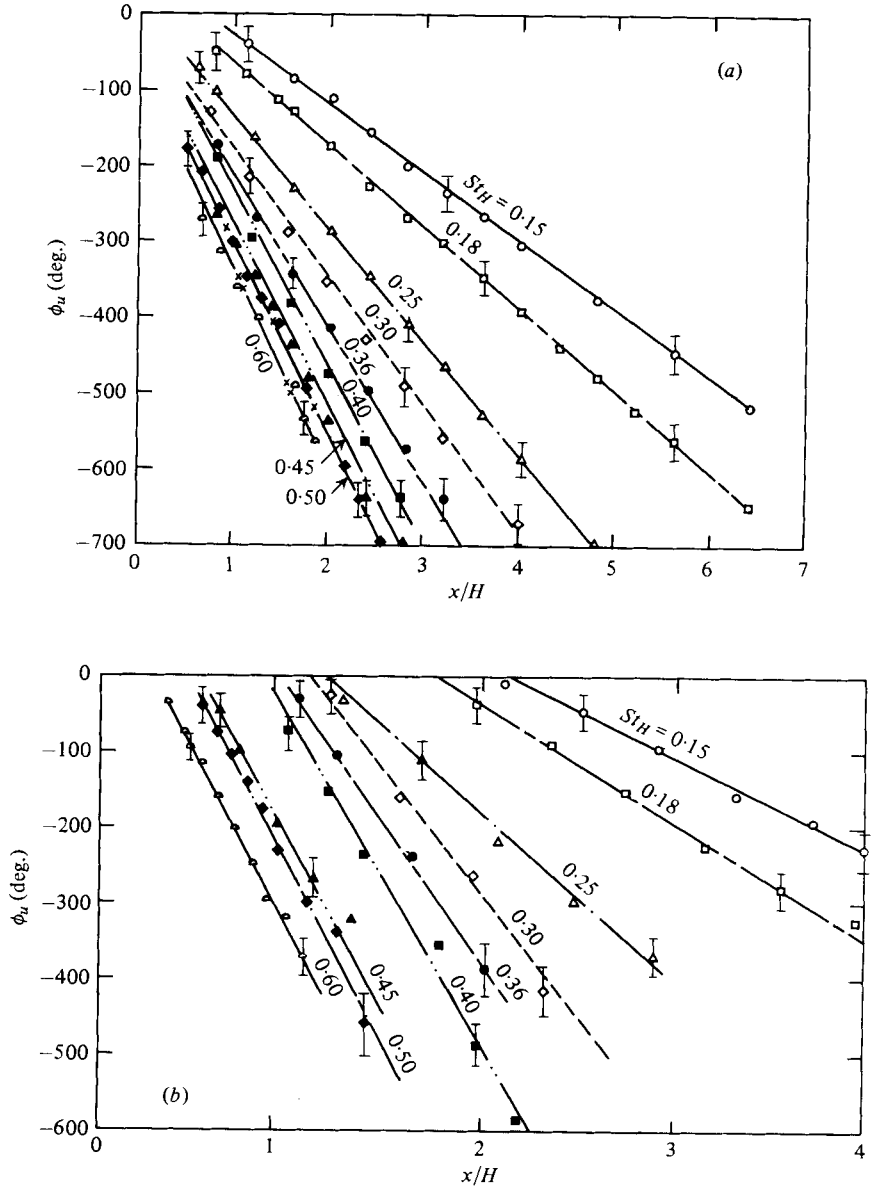

FIGURE 14. Axial variations of ϕ_u at different St_H: (*a*) CL; (*b*) SL. ○, $St_H = 0{\cdot}15$; □, $St_H = 0{\cdot}18$; △, $St_H = 0{\cdot}25$; ◇, $St_H = 0{\cdot}30$; ●, $St_H = 0{\cdot}36$; ■, $St_H = 0{\cdot}40$; ▲, $St_H = 0{\cdot}45$; ◆, $St_H = 0{\cdot}50$; ○, $St_H = 0{\cdot}60$.

neither too far downstream to invalidate the applicability of a free shear-layer theory nor too close to be beyond the range for which the experimental wave eigenvalues were determined (i.e. the x ranges in figures 14*a*, *b*). Michalke solved the inviscid Orr–Sommerfeld equation (also called the Rayleigh equation);

$$(U-c)(D^2-\alpha^2)\phi-(D^2U)\phi=0,$$

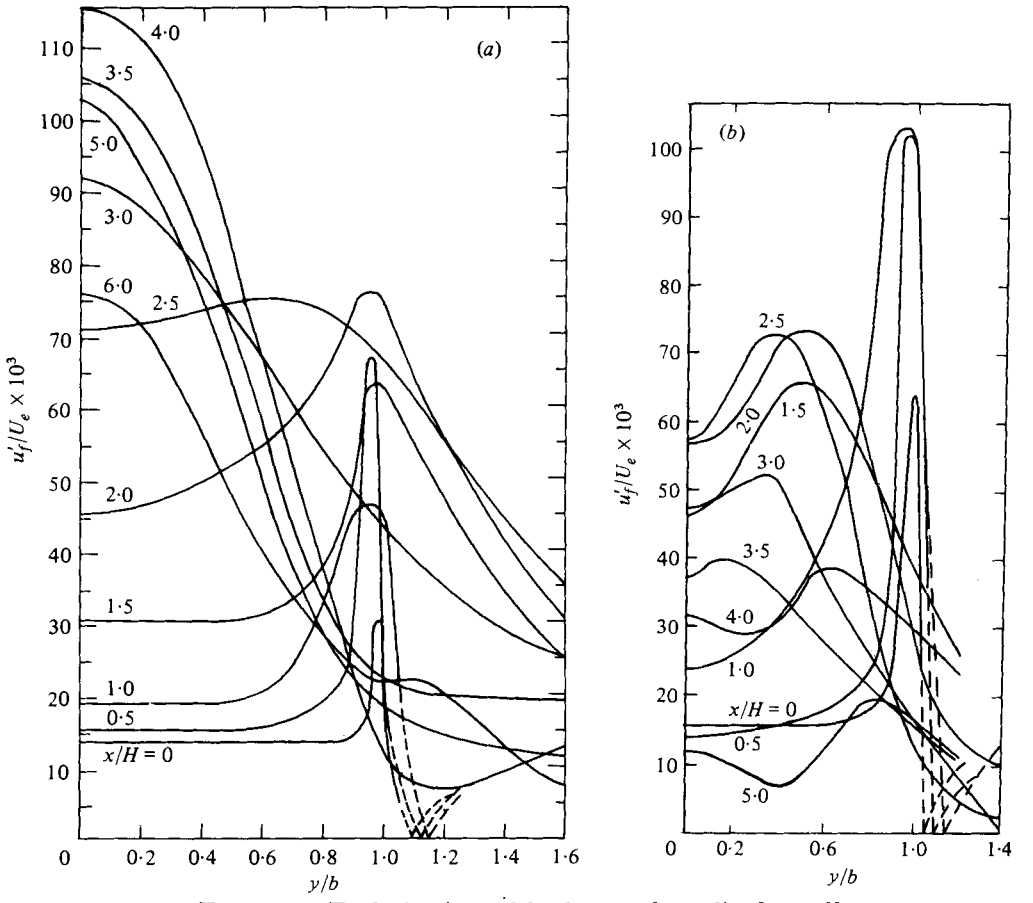

FIGURE 15. Evolution in x of fundamental amplitude profiles: (*a*) $St_H = 0{\cdot}18$; (*b*) $St_H = 0{\cdot}30$.

for the mean velocity profile

$$U(y/L) = 0{\cdot}5U_c[1+\tanh(y/L)];$$

where U_c is the local maximum velocity and L the shear-layer vorticity thickness, i.e.

$$L = U_c/(\partial U/\partial y)_{\max} = \frac{1}{|\omega|_{\max}}\int_{-\infty}^{\infty}|\omega|\,dy.$$

Here $\phi(y)$ is the complex amplitude of the disturbance stream function, $c = c_{\mathscr{R}} + ic_{\mathscr{I}}$ is the complex phase velocity, $\alpha = \alpha_{\mathscr{R}} + i\alpha_{\mathscr{I}}$ is the complex wavenumber and $D = d/dy$. That is,

$$u_f = \tfrac{1}{2}D\phi(y)\exp\{i\alpha(x-ct)\} + \text{conjugate},$$
$$v_f = -\tfrac{1}{2}i\alpha\,\phi(y)\exp\{i\alpha(x-ct)\} + \text{conjugate},$$

so that $u_f' = [(D\phi_{\mathscr{R}})^2 + (D\phi_{\mathscr{I}})^2]^{\frac{1}{2}}$, and $\phi_u = \arctan[D\phi_{\mathscr{I}}/D\phi_{\mathscr{R}}]$.

At the chosen station, i.e. at $x/H = 1$, L was experimentally found to be 0·279 cm and 0·305 cm for $St_H = 0{\cdot}18$ and 0·3, respectively. Using these values, $u_f'(y)$ and $\phi_u(y)$

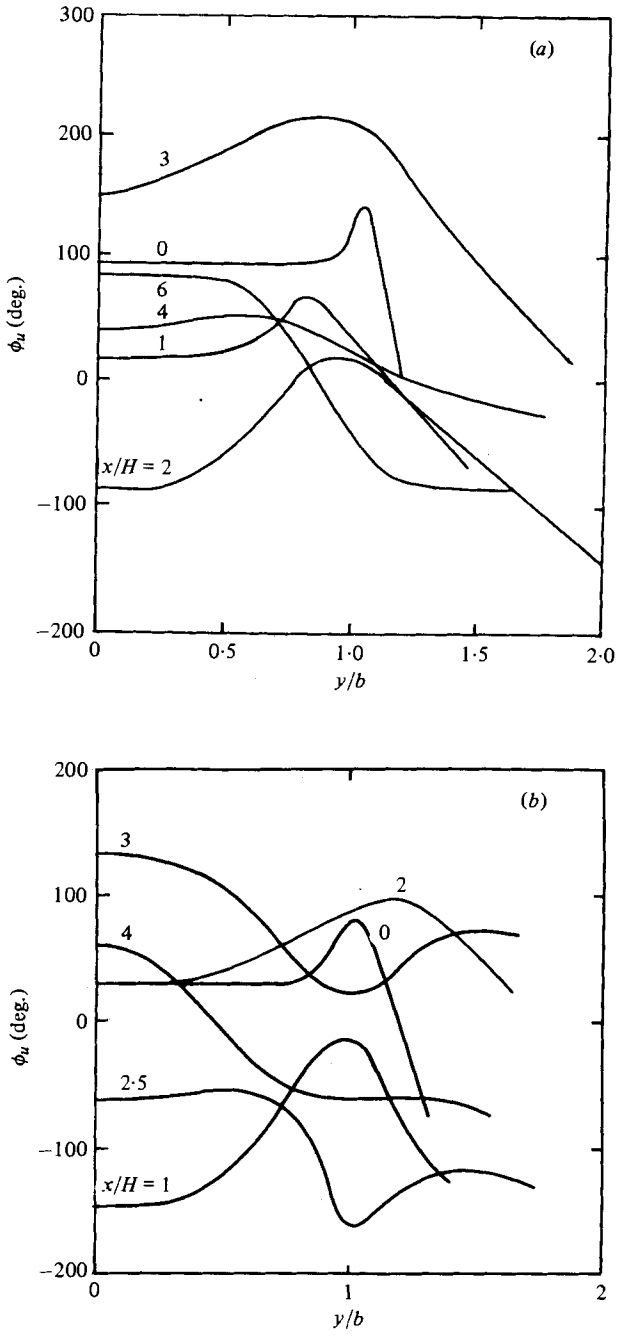

FIGURES 16 (*a*, *b*). For legend see next page.

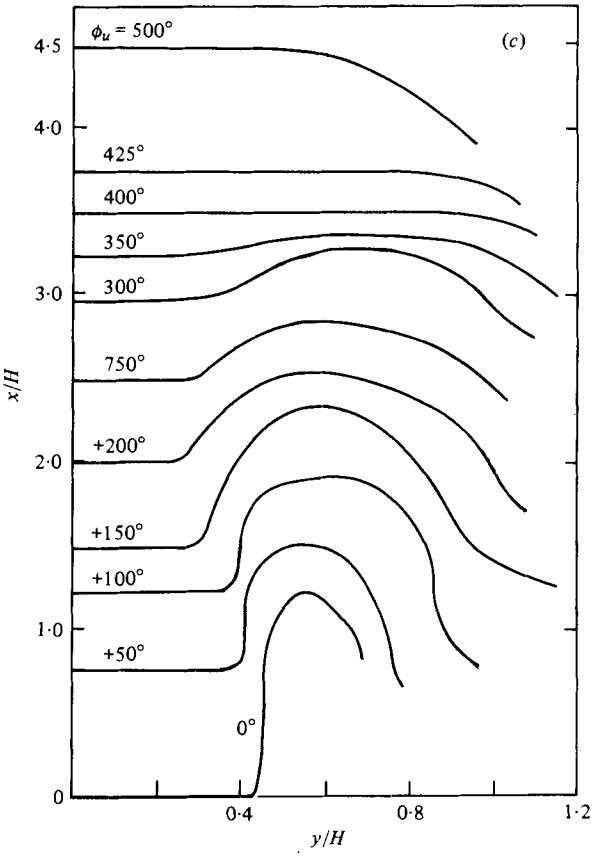

FIGURE 16. Evolution in x of fundamental phase profiles: (*a*) $St_H = 0{\cdot}18$; (*b*) $St_H = 0{\cdot}30$. (*c*) Contours of constant phase ϕ_u: $St_H = 0{\cdot}18$, $u'_{fe}/U_e = 2{\cdot}5\,\%$.

were computed from Michalke's theory. Figures 17(*a*, *b*) show distributions of the measured $u'_f(y/L)$ and $\phi_u(y/L)$ compared with Michalke's theory (1965*b*) for $St_H = 0{\cdot}18$ and $x/H = 1$. Figures 18(*a*, *b*) show the corresponding comparisons for $St_H = 0{\cdot}30$ and $x/H = 1$. The theoretical and experimental amplitude distributions are normalized by the maximum values. In both figures, the dashed lines represent interpreted distributions, because the sensitivity of the lock-in amplifier at the locations of small amplitudes is low. The agreement on the amplitude distributions is quite good. However, the agreement on the ϕ_u data is poor. The phase reversal, i.e. an abrupt 180° jump as predicted by the theory, is not supported by the data. This disagreement is not explainable easily but may be associated with a number of effects not accounted for in the linear, inviscid, laminar, parallel flow theory. Furthermore, the measured mean velocity profile does not agree even closely with the assumed hyperbolic tangent profile. Crighton & Gaster (1976) have shown that the instability of the profile can be altered by small changes in the mean velocity distribution. Some jitter in the arrival of the disturbance at the measurement location would also contribute to smoothing out the jump in the phase profile.

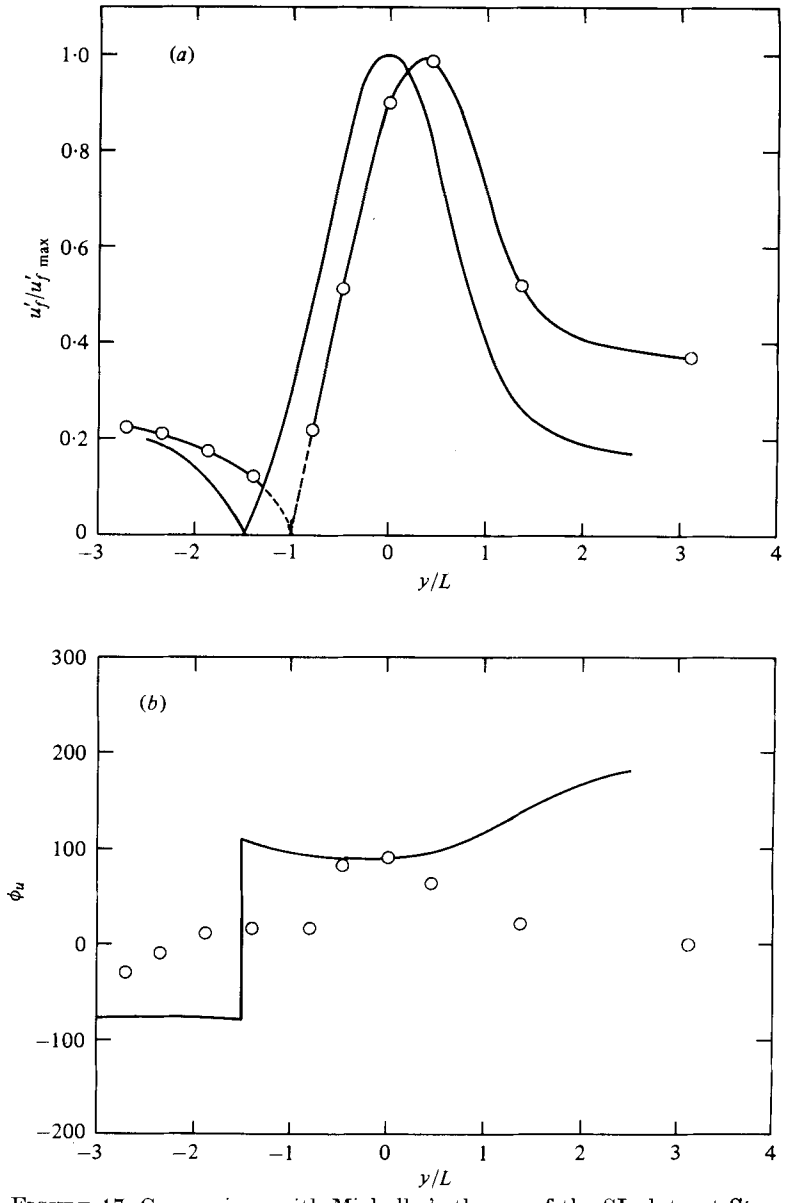

FIGURE 17. Comparison with Michalke's theory of the SL data at $St_H = 0{\cdot}18$ and $x/H = 1{\cdot}0$: (*a*) $u'_f/u'_{f\max}$; (*b*) ϕ_u (deg.).

(*d*) *Wave eigenvalues*

The wave fundamental amplitude and phase profiles show that these do not represent a pure mode. However, for the purpose of approximate analysis and identification of the wave eigenvalues, we will assume the disturbances to represent a single mode and of sufficiently small amplitude to be treated by the linear stability theory. Thus, we can represent the velocity disturbance as

$$u_f = \tfrac{1}{2}\hat{u}(y)\, e^{i\alpha(x-ct)} + \text{conjugate},$$

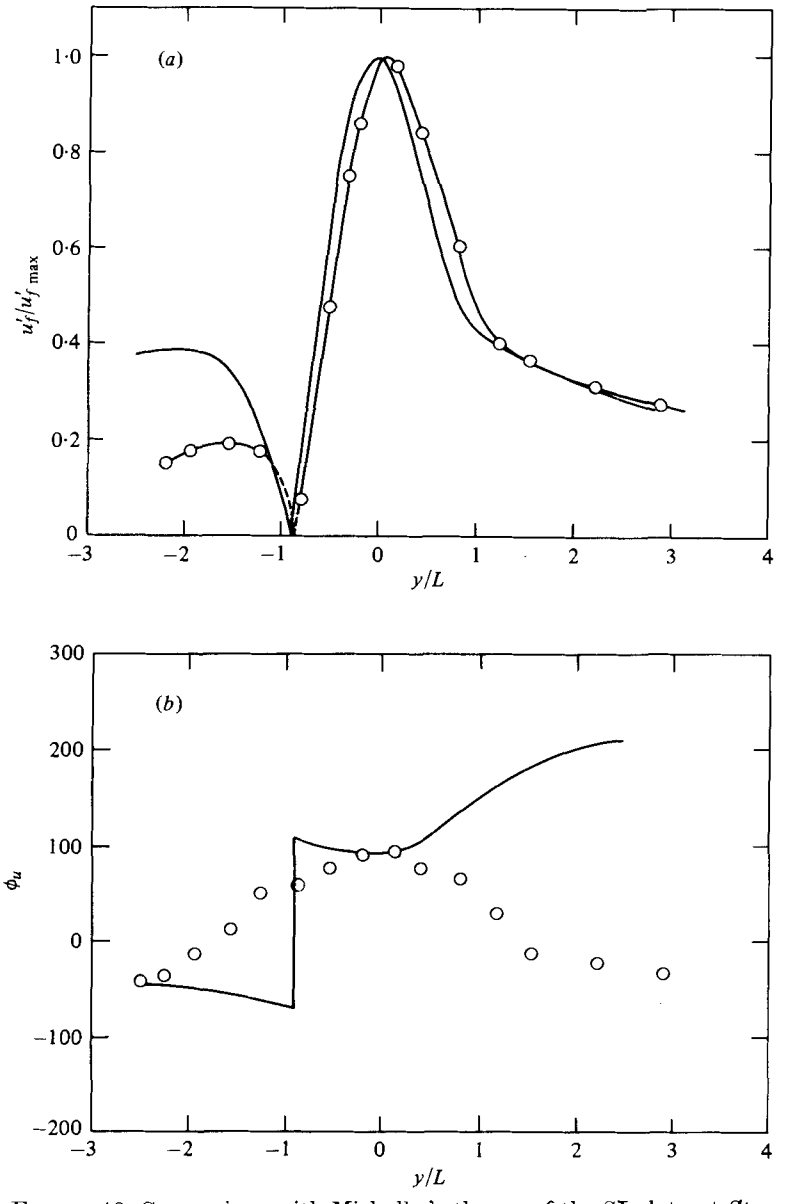

FIGURE 18. Comparison with Michalke's theory of the SL data at $St_H = 0{\cdot}30$ and $x/H = 1{\cdot}0$; (*a*) $u_f'/u_{f\max}'$; (*b*) ϕ_u (deg.).

where u_f is the modulus of the (complex) longitudinal disturbance amplitude. At two streamwise stations x_1, x_2 both at the same y,

$$\frac{u_f(x_2, y, t)}{u_f(x_1, y, t)} = \exp\left[-\alpha_{\mathscr{I}}(x_2 - x_1) + i\alpha_{\mathscr{R}}(x_2 - x_1)\right],$$

$$\left|\frac{u_f(x_2)}{u_f(x_1)}\right| = \exp\left[-\alpha_{\mathscr{I}}(x_2 - x_1)\right] = \frac{u_{f2}'}{u_{f1}'}.$$

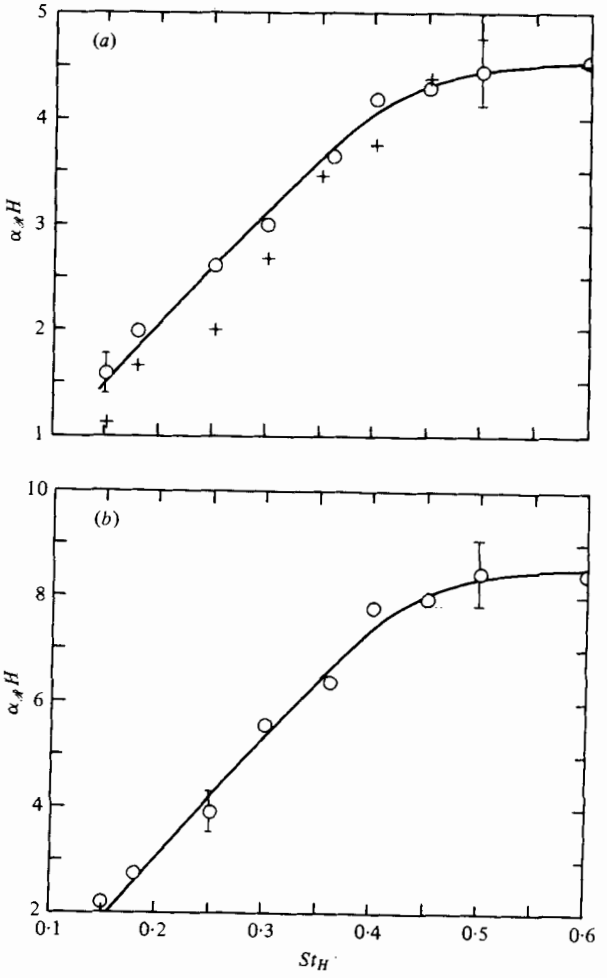

FIGURE 19. Wavenumber dependence on St_H: (*a*) CL; (*b*) SL.

Thus,

$$\alpha_{\mathscr{I}} = \frac{\ln(u'_{j1}/u'_{j2})}{x_2 - x_1}.$$

Also, $\phi_u(x_2, y, t) = \phi_u(x_1, y, t) + \alpha_{\mathscr{R}}(x_2 - x_1)$, and

$$\alpha_{\mathscr{R}} = \frac{\phi_{u2} - \phi_{u1}}{x_2 - x_1}.$$

Consequently, the wavelength λ and the phase velocity are given as

$$\lambda = 2\pi/\alpha_{\mathscr{R}}; \quad V_c = \omega U_e/\alpha_{\mathscr{R}} H,$$

where $\omega = 2\pi St_H$ is the non-dimensional circular frequency.

Figures 19(*a*, *b*) show the dimensionless wavenumber $\alpha_{\mathscr{R}}H$ as a function of St_H on the CL and in the SL, respectively; $\alpha_{\mathscr{R}}$ increases linearly with St_H except near the highest values of St_H. The linear relation between $\alpha_{\mathscr{R}}H$ and St_H suggests that, for the lower St_H range, the plane jet acts as a non-dispersive waveguide. Crow & Champagne's

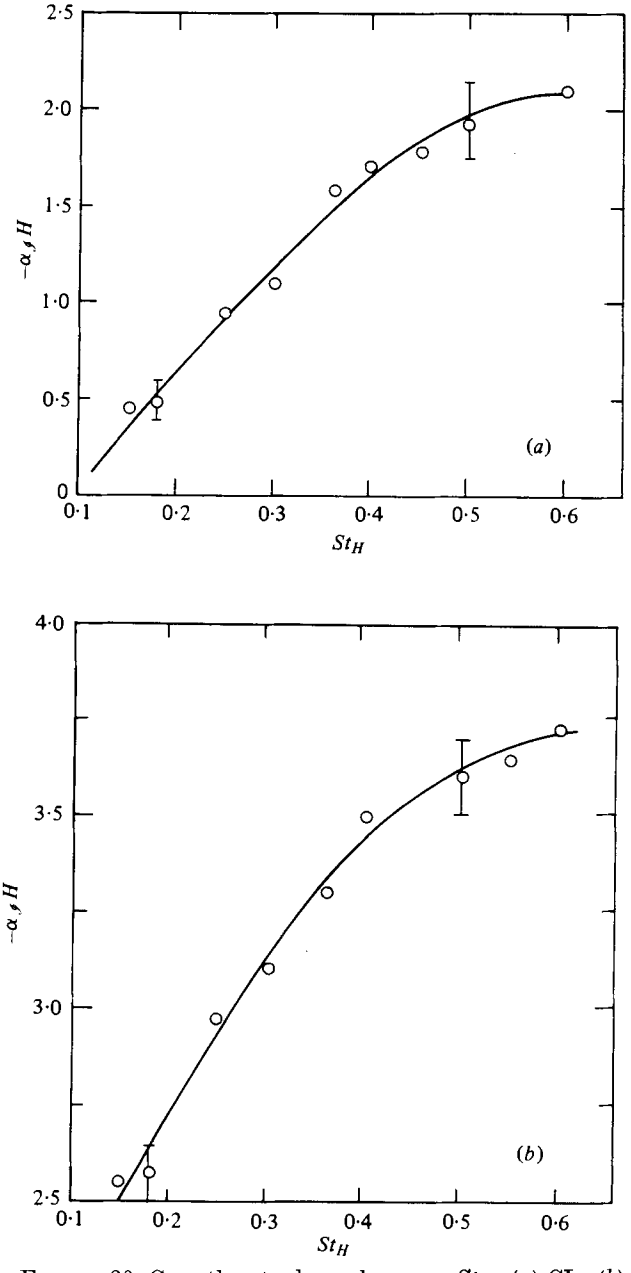

FIGURE 20. Growth-rate dependence on St_H: (*a*) CL; (*b*) SL.

(1971) data are also plotted and show comparable wave behaviour in the circular jet. Numerical solution for the plane jet by Mattingly & Criminale (1971) also gives a linear relation between $\alpha_{\mathscr{R}} H$ and St_H. Figures 20 (*a*, *b*) show the dimensionless spatial growth rate $\alpha_{\mathscr{I}} H$ as a function of St_H for the CL and the SL, respectively. The growth rate also increases with St_H but tends to level off at the highest range of St_H. (Note that $\alpha_{\mathscr{I}} H$ has a larger uncertainty at higher St_H.) Figures 21 (*a*, *b*) show the phase velocity

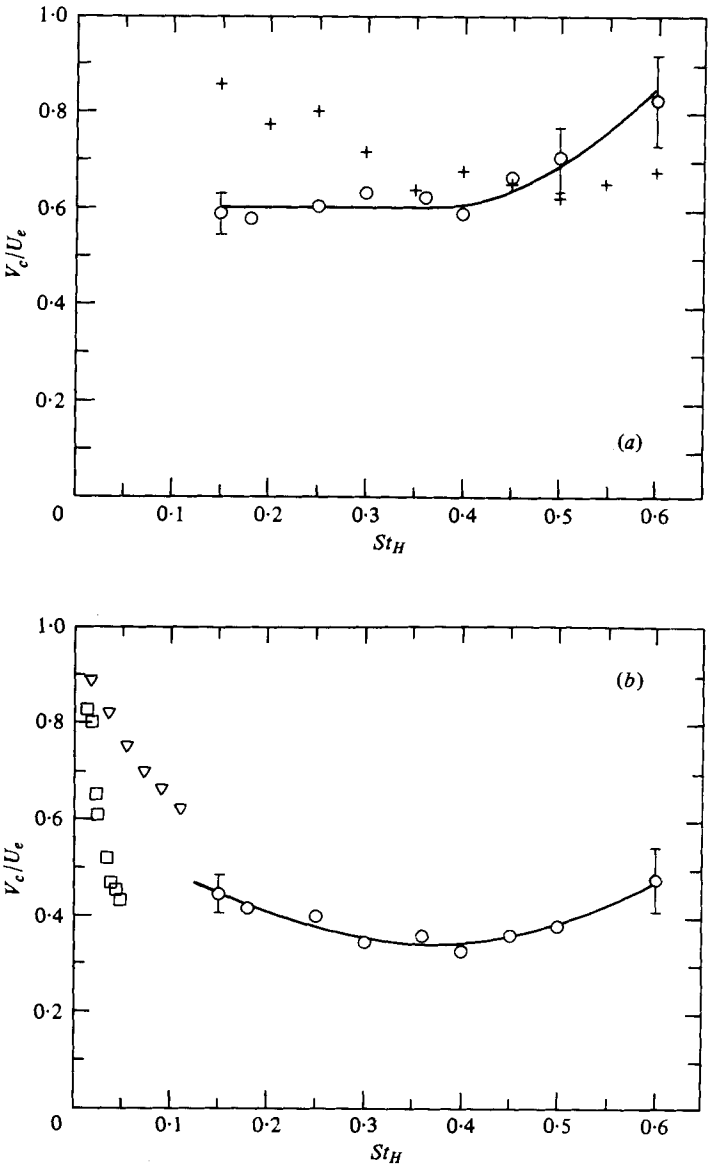

FIGURE 21. (*a*) Variation of V_c with St_H on the centre-line: —○—, present data; +, circular jet data of Crow & Champagne (1971). (*b*) Variation of V_c with St_H in the shear layer: —○—, present data; ▽, Michalke's (1965*b*) theory for a shear layer; □, Mattingly & Criminale's (1971) theory for a fully developed laminar plane jet.

or celerity V_c/U_e as a function of St_H for the CL and SL, respectively. Also included are Crow & Champagne's (1971) data on the circular jet and Michalke's (1965*b*) and Mattingly & Criminale's (1971) theoretical predictions.

Note that the uncertainty in the phase data are higher at locations of smaller fundamental amplitudes due to reduced sensitivity of the lock-in amplifier at low signal levels. Consequently, the uncertainty in the $\alpha_{\mathscr{R}}$, $\alpha_{\mathscr{I}}$, and V_c data are larger at higher St_H, even though scatter of the data does not necessarily suggest so.

5. Concluding remarks

The response of a high-aspect-ratio (44:1) plane air jet to small-amplitude symmetric perturbations of the initial condition was investigated by subjecting the jet to a longitudinal cavity resonance mode, induced by a speaker attached to the settling chamber. Hot-wire measurements were performed in the first few slit-widths of the jet with a top-hat exit profile; the thin-lip boundary layers agree well with the Blasius profile. The amplitude and phase profiles of the fundamental have been educed from the fluctuating signal with a lock-in amplifier, phase-locked to the excitation signal.

The effect of the 1·4 % excitation, covering the Strouhal number range

$$0{\cdot}15 \leqslant St_H \leqslant 0{\cdot}6,$$

on the mean velocity and longitudinal and transverse fluctuation intensities as well as the integral measures like spread rate, mass and momentum fluxes (and thus the entrainment rate) is considerably smaller than that in the circular jet (Crow & Champagne 1971; Zaman & Hussain 1980). These data suggest that the growth of the instability and the resulting vortex roll-up is considerably stronger in the circular jet. If vortex pairing is the primary mechanism controlling entrainment (Winant & Browand 1974; Hussain & Zaman 1975), pairing in the near field of a plane jet is weaker. This, also conjectured before the present experiment was planned, appears reasonable on the ground that vortex merger of the like-signed vortex rings through the leapfrog motion in the circular jet appears much more energetic (Zaman & Hussain 1980) than is likely between the two opposite-signed line vortices near the end of the potential core of a slit jet, even though like-signed line vortices merge separately near each lip. While the vortex rings in the circular jet undergo breakdown before the end of the potential core, primarily though evolution of azimuthal lobe structures (Widnall 1975; Saffman 1978*b*; Hussain & Zaman 1980; Clark 1979), the coherent structure near the exit of the circular jet is well correlated circumferentially. It is not likely that the coherent structure near the exit of a plane jet is well correlated for the entire span.

The induced disturbance initially grows much more rapidly in the shear layer but, further downstream, the amplitude is much larger on the centre-line. The near field of a jet is thus a complex flow, being the overlapping region of two limiting kinds of flows: two shear layers adjacent to the lip and the bell-shaped profile near the end of the potential core. The initial (inviscid) instability of each shear layer occurs first before the instability of the entire jet column takes over. In the circular jet, two corresponding modes: the 'shear-layer mode' and the 'jet-column mode' were also identified (Zaman & Hussain 1980). It is thus not surprising that an instability analysis based on either the shear-layer profile (Michalke 1965*a*, *b*) or an appropriate jet profile (Sato 1960; Crow & Champagne 1971; Mattingly & Criminale 1971) cannot satisfactorily predict the amplitude and phase profiles even in the near field of a jet.

However, making the simplistic assumption that the measured amplitudes and phases correspond to a normal mode, the *average* wave characteristics (i.e. eigenvalues) have been determined along the jet centre-line (CL) and the shear layer (SL). The wavenumber (whose value in the SL is typically twice that on the CL) and the growth

rate (whose value in the SL is higher than that on the CL) increase with St_H, approaching constant values at higher St_H. Note that in view of the rapid change in x of the shape of the fundamental profile $u_f'(y)$ in the shear layer, α_ϕ data in the shear layer can be extremely sensitive to the y-location in the shear layer (Freymuth 1966; Hussain & Zaman 1978). The phase velocity on the centre-line is higher than in the shear layer. Data show that at the lower ranges of St_H the near-field plane jet acts as a non-dispersive waveguide.

Sato found reasonably close agreement of his data (for antisymmetric acoustic excitation) with the temporal theory by assuming that predictions from the temporal theory is equivalent to a spatially dependent wave if the co-ordinates are convected downstream with the disturbance phase velocity. This assumption of equivalence was made by many investigators (for example, Schubauer & Skramstad (1947) in interpreting boundary-layer transition experiments) until Gaster (1962) showed its severe restrictiveness.

Because of these considerations, we compared our data with the spatial theories. However, Crow & Champagne's (1971) data in the circular jet showed good agreement with the temporal theory. Also, Freymuth's (1966) wave eigenvalue data in the shear layers of plane and circular jets agreed with the spatial theory in the lower Strouhal-number range, but with the temporal theory in the higher Strouhal-number range. These peculiarities of the theory have not yet been explained by the theoreticians. The present results should encourage improvement of theoretical predictions as well as serve as a calibrator of newer theories.

Parenthetically, recognizing some of the limitations of the shear wave representation of the jet near-field flow structure, investigations based on flow-visualization and conditionally sampled hot-wire measurements were started in parallel (Zaman & Hussain 1980; Hussain & Zaman 1975, 1980; Sokolov *et al.* 1980; Clark 1979). It is believed that these two complementary approaches have unveiled significant new information on the physics of jet flows.

The authors are grateful to Dr K. B. M. Q. Zaman and Dr S. J. Kleis for their help in various forms. This research was funded by the National Science Foundation under the initiation Grant NSF-GK-23626 and the Office of Naval Research under Grant NR 062-480.

REFERENCES

Antonia, R. A., Chambers, A. J. & Hussain, A. K. M. F. 1980 *Phys. Fluids* **23**, 695.

Batchelor, G. K. 1970 *An Introduction to Fluid Dynamics*. Cambridge University Press.

Beavers, G. S. & Wilson, T. A. 1970 *J. Fluid Mech.* **44**, 97.

Bechert, D. & Pfizenmaier, E. 1975 *J. Sound Vib.* **43**, 581.

Bradshaw, P. 1977 *J. Fluid Mech.* **80**, 795.

Browand, F. K. & Laufer, J. 1975 *Turbulence in Liquids*, vol. 5, p. 333. University of Missouri-Rolla.

Brown, G. L. & Roshko, A. 1974 *J. Fluid Mech.* **64**, 775.

Bruun, H. H. 1977 *J. Fluid Mech.* **64**, 775.

Cantwell, B., Coles, D. & Dimotakis, P. 1978 *J. Fluid Mech.* **87**, 641.

Chan, Y. Y. 1976 *Phys. Fluids* **19**, 2042.

Clark, A. R. 1979 Ph.D. dissertation, University of Houston.

CRIGHTON, D. G. & GASTER, M. 1976 *J. Fluid Mech.* **77**, 397.

CROW, S. C. & CHAMPAGNE, F. H. 1971 *J. Fluid Mech.* **49**, 547.

FREYMUTH, P. 1966 *J. Fluid Mech.* **25**, 683.

GASTER, M. 1962 *J. Fluid Mech.* **14**, 227.

GOLDSCHMIDT, V. W. & BRADSHAW, P. 1973 *Phys. Fluids* **16**, 354.

GOLDSCHMIDT, V. W. & KAISER, K. F. 1971 *A.I.Ch.E. Chem. Eng. Symp. Ser.* **67**, 91.

GUTMARK, E. & WYGNANSKI, I. 1976 *J. Fluid Mech.* **73**, 465.

HASAN, M. A. Z. 1978 M.S. thesis, University of Houston.

HILL, B. J. 1972 *J. Fluid Mech.* **51**, 773.

HUSSAIN, A. K. M. F. & CLARK, A. R. 1977 *Phys. Fluids* **20**, 1416.

HUSSAIN, A. K. M. F., KLEIS, S. J. & SOKOLOV, M. 1980 *J. Fluid Mech.* **98**, 97.

HUSSAIN, A. K. M. F. & RAMJEE, V. 1976 *Trans. A.S.M.E.* I, *J. Fluids Engng* **98**, 58.

HUSSAIN, A. K. M. F. & REYNOLDS, W. C. 1970 *J. Fluid Mech.* **41**, 241.

HUSSAIN, A. K. M. F. & ZAMAN, K. B. M. Q. 1975 *Proc. 3rd Int. Symp. on Univ. Res. in Transportation Noise*, p. 314. University of Utah.

HUSSAIN, A. K. M. F. & ZAMAN, K. B. M. Q. 1978 *J. Fluid Mech.* **87**, 349.

HUSSAIN, A. K. M. F. & ZAMAN, K. B. M. Q. 1980 *J. Fluid Mech.* (to appear).

HUSSAIN, A. K. M. F. & ZEDAN, M. F. 1978 *Phys. Fluids* **21**, 1100.

KLEIS, S. J. 1974 Ph.D. thesis, Michigan State University.

KOTSOVINOS, N. E. 1976 *J. Fluid Mech.* **77**, 305.

KOVASZNAY, L. S. G. 1978 *Structure and Mechanisms of Turbulence I* (ed. H. Fiedler), Lecture Notes in Physics, vol. 75, p. 1. Springer.

LANDAHL, M. T. 1967 *J. Fluid Mech.* **29**, 441.

LAU, J. C. & FISHER, M. J. 1975 *J. Fluid Mech.* **67**, 299.

MATTINGLY, G. E. & CRIMINALE, W. O. 1971 *Phys. Fluids* **14**, 2258.

MICHALKE, A. 1965*a* *J. Fluid Mech.* **22**, 351.

MICHALKE, A. 1965*b* *J. Fluid Mech.* **23**, 521.

MOFFATT, H. K. 1968 *Computation of Turbulent Boundary Layers* – 1968 *AFOSR IFP–Stanford Conf.*, p. 495. Stanford University.

MOLLO-CHRISTENSEN, E. 1967 *Trans. A.S.M.E.* E, *J. Appl. Mech.* **89**, 1.

MOORE, C. J. 1977 *J. Fluid Mech.* **80**, 321.

MORKOVIN, M. V. & PARANJAPE, S. V. 1971 *Z. Flugwiss.* **19**, 328.

MORRISON, W. R. B. & KRONAUER, R. E. 1970 *J. Fluid Mech.* **39**, 117.

PAYNE, F. R. & LUMLEY, J. L. 1967 *Phys. Fluids* **10**, S194.

PETERSEN, R. A., KAPLAN, R. E. & LAUFER, J. 1974 *N.A.S.A. Contractor Rep.* no. 134733.

PHILLIPS, O. M. 1967 *J. Fluid Mech.* **29**, 131.

REYNOLDS, W. C. & HUSSAIN, A. K. M. F. 1972 *J. Fluid Mech.* **52**, 263.

RICOU, F. P. & SPALDING, D. B. 1961 *J. Fluid Mech.* **11**, 21.

ROCKWELL, D. O. 1972 *Trans. A.S.M.E.* E, *J. Appl. Mech.* **39**, 883.

ROCKWELL, D. O. & NICCOLLS, W. O. 1972 *Trans. A.S.M.E.* D, *J. Basic Engng* **94**, 720.

SAFFMAN, P. G. 1978*a* *Structure and Mechanisms of Turbulence II* (ed. H. Fiedler), Lecture Notes in Physics, vol. 76, p. 273. Springer.

SAFFMAN, P. G. 1978*b* *J. Fluid Mech.* **84**, 625.

SATO, H. 1960 *J. Fluid Mech.* **7**, 53.

SCHUBAUER, G. B. & SKRAMSTAD, H. K. 1947 *J. Aero. Sci.* **14**, 69.

SOKOLOV, M., HUSSAIN, A. K. M. F., KLEIS, S. J. & HUSAIN, Z. D. 1980 *J. Fluid Mech.* **98**, 65.

THOMPSON, C. A. 1975 Ph.D. dissertation, University of Houston.

TOWNSEND, A. A. 1956 *The Structure of Turbulent Shear Flow.* Cambridge University Press.

VLASOV, Y. V. & GINEVSKIY, A. S. 1974 *N.A.S.A.* TTF-15,721.

WIDNALL, S. 1975 *Ann. Rev. Fluid Mech.* **7**, 141.

WILLS, J. A. B. 1964 *J. Fluid Mech.* **20**, 417.

WINANT, D. D. & BROWAND, F. K. 1974 *J. Fluid Mech.* **63**, 237.
WYGNANSKI, I. & GUTMARK, E. 1971 *Phys. Fluids* **14**, 1309.
WYGNANSKI, I., SOKOLOV, M. & FRIEDMAN, D. 1976 *J. Fluid Mech.* **78**, 785.
YULE, A. J. 1978 *J. Fluid Mech.* **89**, 413.
ZAMAN, K. B. M. Q. & HUSSAIN, A. K. M. F. 1980 *J. Fluid Mech.* (to appear).